DOE-ER-0313/33
Distribution
Categories
UC-423, -424

FUSION MATERIALS
SEMIANNUAL PROGRESS REPORT
FOR THE PERIOD ENDING
December 31, 2002

Prepared for
DOE Office of Fusion Energy Sciences
(AT 60 20 10 0)

DATE PUBLISHED: MARCH 2003

Prepared for
OAK RIDGE NATIONAL LABORATORY
Oak Ridge, Tennessee 37831
Managed by
U.T.-Battelle, LLC
For the
U.S. DEPARTMENT OF ENERGY

FOREWORD

This is the thirty-third in a series of semiannual technical progress reports on fusion materials science activities supported by the Fusion Energy Sciences Program of the U.S. Department of Energy. This report focuses on research addressing the effects on materials properties and performance from exposure to the neutronic, thermal, and chemical environments anticipated in the chambers of fusion experiments and energy systems. This research is a major element of the national effort to establish the materials knowledge base of an economically and environmentally attractive fusion energy source. Research activities on issues related to the interaction of materials with plasmas are reported separately.

The results reported are the product of a national effort involving a number of national laboratories and universities. A large fraction of this work, particularly in relation to fission reactor irradiations, is carried out collaboratively with partners in Japan, Russia, and the European Union. The purpose of this series of reports is to provide a working technical record for the use of program participants, and to provide a means of communicating the efforts of fusion materials scientists to the broader fusion community, both nationally and worldwide.

This report has been compiled and edited under the guidance of Ron Klueh and Renetta Godfrey, Oak Ridge National Laboratory. Their efforts, and the efforts of the many persons who made technical contributions, are gratefully acknowledged.

S. E. Berk
Facilities and Enabling Technologies Division
Office of Fusion Energy Sciences

TABLE OF CONTENTS

1.0 VANADIUM ALLOYS

STRONGLY NON-ARRHENIUS INTERSTITIAL DIFFUSION IN VANADIUM – S. Han, R. Car, and D. J. Srolovitz (Princeton University), L. A. Zepeda-Ruiz (LLNL),

OBJECTIVE

Self-interstitial atoms (SIA), produced in the irradiation of metals, are key components of the micro-structural evolution of the material. The microstructural evolution of the irradiated material is largely determined by the migration, clustering, and annihilation of the SIAs. The objective of this research is to study self-diffusion via SIA migration in pure vanadium through a multiscale computational study.

SUMMARY

We perform molecular dynamics simulation to study the diffusion of SIAs in vanadium. The interatomic potentials employed were developed by fitting to first-principle, quantum mechanical results on SIA structure and energetics. The present results demonstrate that the SIA in vanadium exists in a <111>-dumbbell configuration and migrates along <111> directions, in agreement with first-principles calculations. At low and intermediate T, the diffusion is one-dimensional, but at higher temperatures, the dumbbell can rotate into other <111> directions, resulting in three-dimensional at high T. The apparent activation energy for migration increases with temperature as a result of a complex correlation effect even at temperatures before significant dumbbell reorientation occurs.

INTRODUCTION

Vanadium alloys are important candidate materials for future fusion reactors. Although it is the evolution of point defect distribution that determine the ultimate lifetime of these materials, there have been very few reliable experimental or theoretical studies of the fundamental point defect properties in vanadium. Earlier experiments have shown that SIA diffusion occurs down to temperatures as low as~4K with a migration energy of less than 0.01 eV. Extensive computer simulation studies of radiation damage in other metals have been performed. For example, simulations of bcc Fe have shown that SIAs and SIA clusters (small, perfect dislocation loops) are created along close-packed directions and tend to migrate along specific crystallographic directions. In these materials, the SIAs lie in <110> directions but rotate into the <111> in order to migrate. The resulting diffusion occurs via migration in a <111> direction, relaxation into a stable <110> orientation and then rotation into another <111> directions; this yields a 3D random walk diffusional trajectory with an Arrhenius temperature dependence with a very low activation energy, usually ~0.1 eV. Simulation studies of SIA migration have also been performed for V. These show that SIA migration in V is very similar to that in Fe. Unfortunately, these are not consistent with our own first principles calculations, which clearly demonstrate that the stable SIA structure in V is a <111> oriented dumbbell, rather than the <110> oriented dumbbell in Fe. Given this fundamental discrepancy, we are forced to conclude that SIA migration in Fe and V are fundamentally different and SIA diffusion in V is poorly understtod. Therefore, we have undertaken a study of SIA migration in V using our new interatomic potential, which is designed to ensure consistency with the first principles calculations.

COMPUTATIONAL METHOD

The diffusion of individual SIAs in vanadium was investigated using the molecular dynamics (MD) simulation code MDCASK using a new parameterization of a Finnis-Sinclair/EAM potential for vanadium. The reparameterization was performed in order to ensure that the point defect properties were consistent with the predictions of our first-principles calculations that suggest that the most stable SIA is a <111>-dumbbell, which is nearly degenerate with the crowdion configuration. The resultant potential has been extensively tested and successfully used to calculate static point-defect properties in vanadium.

All simulations were performed with a cubic system of 16000 + 1 mobile atoms ($20a_0$x$20a_0$x$20a_0$ computational cell; a_0=3.03Å), with periodic boundary conditions. Simulations were run at temperatures between 100 and 1600 K. The SIA was introduced in the form of a stable <111>-dumbbell followed by a

10 ps equilibration run using a constant temperature ensemble (N,V,T). The simulation was then switched to a microcanonical ensemble (N, V,E) in order to study the SIA migration dynamics. Because of the highly correlated nature of interstitial diffusion, long runs (1 ns) were required to ensure that the reliable diffusivites could be extracted. numerical convergence.

In order to calculate diffusivities, we followed the procedure employed by Guinan *et al*. The total run time is partitioned in *m* intervals of equal duration time τ, and within each the average interstitial positions and orientations determined at intervals $\Delta\tau$. The latter is chosen to ensure that the individual measurements were uncorrelated. This procedure allows us to calculate *D* as the average of all D_i calculated in each segment as

$$D = \frac{1}{m}\sum_{i=1}^{m} D_i$$
$$= \frac{1}{m}\sum_{i=1}^{m} \frac{\langle R^2 \rangle}{2d\tau_i}$$

where $\langle R^2 \rangle$ is the mean squared distance from beginning to end of a trajectory over the time period τ and *d* is the dimensionality of the diffusion path (1D or 3D). In order to assure consistency of the procedure, τ was varied from 5 to 100 ps with $\Delta\tau$ = 1ps. The activation energy and pre-exponential for the diffusivity were obtained via least square fits to the logarithm of the diffusivity vs. 1/*T*.

RESULTS

In order to investigate the migration mechanism of SIA in V, we first analyzed the interstitial trajectories as a function of temperature. Representative trajectories of the SIA center of mass are shown in Figure 1.

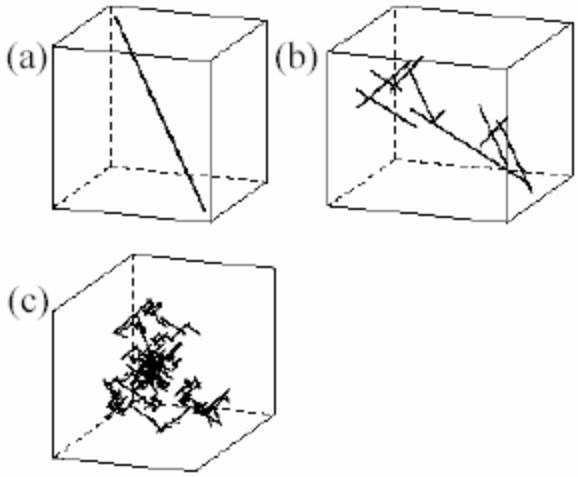

Figure 1: Typical trajectories of migrating SIAs at three different temperatures: (a) T = 100K, (b) T = 700K, and (c) T = 1300K.

We analyzed each trajectory to determine the migration mechanism and type of interstitial. For each temperature, more than 1000 jumps were observed. The interstitial migration mechanism was found to be temperature dependent. For low and intermediate temperatures (100-600 K) the SIA executes an essentially 1D random walk along a <111>-direction, as shown in Fig. 1(a). As temperature increases to T~700K, the SIA begins to make infrequent rotations from one <111>- to a different <111>-direction (passing through a <110>-dumbbell configuration). This results in a 3D trajectory that consists of long 1D

random walk segments with abrupt reorientations, as seen in Fig. 1(b). At very high temperatures, the rotation events become very frequent, such that the SIA is performing a truly 3D random walk (as shown in Fig. 1(c)). Although these results are similar to those reported for other bcc metals (i.e., Fe and Mo), it is fundamentally different. This difference is associated with the stable form of the interstitial - <111>-dumbbell in V and <110>-dumbbell in Fe and Mo. In the Fe and Mo cases, the reorientation or rotation events were associated with the relaxation of the dumbbells from their migration orientations <111> into their stable orientations <110>. Such relaxation events do not occur in the present V case, since the <111>-dumbbell is both the stable and migration form of the SIA. In fact, the <110>-dumbbell orientation corresponds to the saddle point in the V SIA rotation from one <111> orientation to another.

To obtain a more detailed understanding of SIA migration, we monitored the frequency for rotation from one <111>- to any other <111>-direction. Figure 2 shows the rotation frequency vs. $1/k_BT$ for temperatures between 700 and 1600 K (for T < 600K, no rotations were observed).

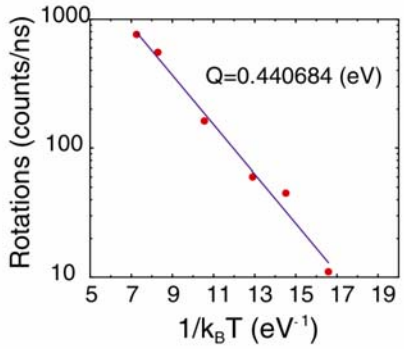

Fig. 2: Arrhenius plot of the SIA rotation frequency.

The logarithm of the rotation frequency is a linear function of the inverse temperature. This suggests that rotation is a thermally activated (Arrhenius) process. The activation energy obtained from Fig. 2, E_m=0.42eV, is consistent with first principles calculations and static calculations using the new interatomic potential which predict a rotational barrier for SIAs in V of 0.35 and 0.4 eV, respectively. The pre-exponential factor obtained from the fit was D_0=1.67x10^{13} rotations/s.

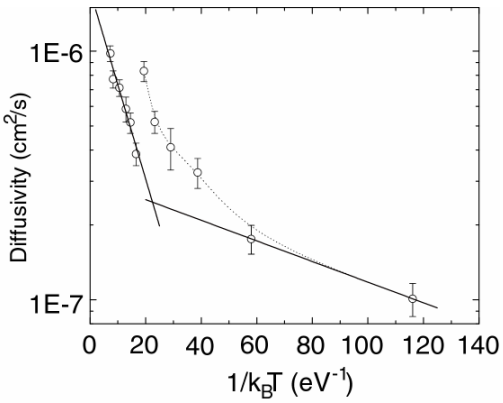

Fig. 3: Arrhenius plot of the SIA diffusion

The diffusivities, *D*, were obtained as described above over a range of temperatures. The results are shown in Fig. 3. Since we observe no rotations below 700K, we assume that the d=1 below 700K and d=3 above 700K. This switch in the value of d used in the determination of D is responsible for the abrupt

drop in D at 700K observed in Fig. 3. The data clearly show that the diffusivity is an Arrhenius function of temperature at high T and at low T, with a continuous transition from a low activation energy at low T to a higher activation energy at elevated T. For low temperatures we obtain D_0=3.0594x10^{-7} cm^2/s and E_m=0.0095 eV. This is in agreement with experimental data that shows that interstitial diffusion in V occurs even at 4 K with a migration energy < 0.01 eV. For high temperatures, we obtained D_0=1.7504x10^{-6} cm^2/s and E_m=0.0872 eV. We observe that at intermediate temperatures (200K < T < 600 K), *D* increases with T. This is interesting because the SIA undergo **NO** rotations during the course of this simulation until T is raised to 700K or above.

DISCUSSION AND CONCLUSION

The presence of a nonlinear regime in the Arrhenius diagram for temperatures between 200 and 600 K is surprising. As discussed above, previous studies of SIA migration in bcc metals showed that SIA migration is a multiple step process that involves not only translation of <111>-oriented dumbbells along a <111>-direction, but also rotations from the stable <110>- to <111>-oriented dumbbells. One could argue that the non-linearity observed in Fig. 3 is a result of the competition (over a certain temperature regime) of these thermally activated processes. But this is clearly not the situation in the case of V. As shown in Fig. 2 no changes in <111>-dumbbell orientation were observed for T< 700 K, *i.e.* SIA migration was purely 1D. Furthermore, analysis of atomic coordinates showed that in this temperature regime, the SIA exists only in a <111>-oriented dumbbell with only small angular deviations (these can be substantial at T~600 K. These deviations are consistent with first-principles results which show that the <111>-dumbbell configuration is stable relative to other dumbbell orientations, but the dumbbell energy varies slowly with misorientation around the <111>-orientation.

Since we have demonstrated that the transition from 1D to 3D diffusion is not responsible for the change in the apparent activation energy for SIA diffusion in V, we must look for another explanation. This can be found in the correlation factor for diffusion. Detailed examination of the SIA trajectories in V shows that SIA hops are correlated. At low temperature, the SIA has a higher probability of jumping back in the direction from whence it came, rather than forward along the same trajectory. We quantified this observation by measuring a correlation factor for SIA diffusion ψ, defined as

$$\psi = \frac{1}{m}\sum_{i=1}^{m}\sigma_i\sigma_{i+1}$$

where σ_i=1 if the SIA moves to the “left” and σ_i=-1 if the SIA moves in towards the “right”. In this way, a value of ψ=1 would mean that the SIA executed *m* jumps all in the same direction, a value of ψ=-1 would mean that the SIA jumps in the opposite direction than its previous jump, and a value of ψ=0 implies an uncorrelated random walk. A plot of ψ as a function of temperature is shown in Fig. 4.

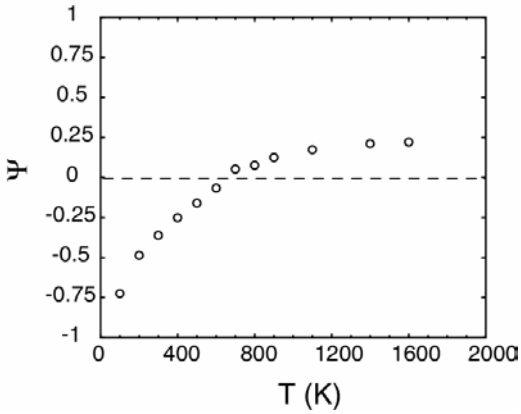

Fig. 4: Correlation factor versus temperature.

From this, we observe that at low T the SIA tends to jump back in the direction from whence it came, while at high T the random walk is more nearly perfect. At high T, there is a slight tendency for the hops to continue in the same direction (e.g.,, a small number of multiple site hops). At low T the SIA has very little thermal energy and hence tends to "bounce off" the next atom and return to its previous position while at high T the higher thermal energy gives rise to a 1D collision cascade. Thus, the non-Arrhenius behavior is not from competing thermally activated events as reported in Fe or Mo, but rather from a temperature-dependent correlation factor.

FABRICATION OF CREEP TUBING FROM THE US AND NIFS HEATS OF V-4Cr-4Ti – A.F. Rowcliffe, (Oak Ridge National Laboratory), W.R. Johnson (Rocket Science & Materials Engineering Services), D.T. Hoelzer (Oak Ridge National Laboratory)

OBJECTIVE

Utilize commercial–scale processing to fabricate small-diameter, thin-wall tubing from plate stock of V-4Cr-4Ti for both the US program heat no.832665 and the NIFS –HEAT-2 and produce sufficient tubing to meet foreseeable programmatic needs for investigating creep behavior in both lithium and vacuum environments and for carrying out irradiation creep measurements

SUMMARY

Commercial-scale fabrication of thin-walled tubing for thermal and irradiation creep testing of V4Cr-4Ti has been initiated at Century Tubes Inc, San Diego. In an effort to minimize the occurrence of the surface flaws and cracks which characterized the previous batch of tubing, the technical specifications have been extensively modified. In particular improvements have been made in the cleaning procedures and in the control of the vacuum during all stages of the annealing cycle; the levels of cold work applied during the final stages have been substantially reduced. Both the US program heat and the Japanese NIFS-HEAT-2 are being processed; interim examination shows significant increases in oxygen content for both heats in spite of the added precautions introduced. Surface defects similar to those observed in the previous batch of tubing were detected in one section of tubing from the US heat after 4 draw cycles while the NIFS heat was relatively free of surface defects.

PROGRESS AND STATUS

Introduction

The pressurized tube creep specimens adopted by the US and Japanese programs measures 25.4 mm long with a 4.57mm outside diameter, and a wall thickness of 0.25mm. In 1995, Argonne National Laboratory coordinated a campaign to fabricate ~ 6 meters of tubing from the US program heat no 832665 with Century Tubes Inc of San Diego as the primary contractor [1]. This campaign met with mixed success with a large fraction of the tubing developing cracks on both the inside and outside surfaces. These cracks were frequently linked together through the wall thickness. Since they were long enough to be visible to the naked eye, it was possible to select relatively sound segments of tubing to prepare a sufficient number of creep specimens to meet short term program needs. This tubing was used for an initial series of testing both in vacuum and in lithium environments [2] and also used to develop preliminary irradiation creep data in experiments conducted in the ATR[1] and in the HFIR [3]. It was also found that during processing, the level of interstitials elements increased significantly, with carbon increasing from 80 to 300 wppm, oxygen increasing from 310 to 700 wppm and nitrogen going from 85 to 95 wppm, a total increase in interstitial level of ~130%. The increase in oxygen was of particular concern since creep rate is sensitive to oxygen concentration in this range. However, in subsequent creep measurements using this tubing it was observed that the oxygen content decreased to ~100wppm in approx. 1500hrs during tests carried out at 800ºC in a Li environment. Thus it is not entirely clear that the in-Li creep data were compromised by the initially high oxygen level of the ANL batch of tubing since the oxygen concentration reverted to very low levels during testing. However, it has been suggested that the presence of the defects in the tube wall could be responsible for inconsistencies in the measured strains to failure [2].

Two small heats of V-4Cr-4Ti with low levels of interstitials have been produced in Japan under the direction of the National Institute for Fusion Science (NIFS). A small quantity of creep tubing was prepared from the NIFS-HEAT -2 material using a three-directional rolling process [4]. Problems were also encountered in the NIFS campaign with interstitial pick-up and the development of surface defects. Based upon the processing records from the previous batch of tubing from the US heat and

the experience gained from processing the NIFS heat, a new procedure was developed which incorporated a series of changes designed to minimize interstitial pick-up, improve initial surface quality, and to reduce the probability of surface cracking by reducing stress levels in the final drawing stages. Using the new procedure, fabrication of ~10 meters of finished tubing from both heats was initiated at Century Tubes in April 2003.

This report documents the new procedures and discusses the status of the tubing fabrication as it enters the final stages; a full evaluation of the finished tubing will be presented in the next semi-annual report.

Previous Tubing Fabrication Experience

US HEAT 832665

Tubing from the first campaign at Century Tube (subsequently referred to as Batch A tubing) has been used to provide the initial sets of biaxial creep data in vacuum, lithium, and lithium plus neutron radiation environments. During the final stages of drawing and sinking, difficulties were experienced with surface cracking and sometimes complete fracture of tubes. Metallography of several sections was carried out at ORNL. Five out of six randomly selected sections of tubing contained branching cracks at both the ID and OD surfaces penetrating inwards to depths from 20 to 200 microns**.** Longitudinally, these cracks extended from 2 to 200mm in length and so were often visible to the naked eye. Cracks penetrating from both surfaces were often connected by a band of severe macroscopic deformation in which grains were rotated and elongated in a direction 45 degrees to the through –wall radial direction as shown in Fig.1. Many smaller cracks simply penetrated 10-20 microns in from both surfaces. Chemical analysis of the finished tubing indicated that the carbon and oxygen concentrations increased during processing by 220 wppm and 389 wppm respectively. Because archival samples were not secured at each drawing stage it is not possible to say when the cracks developed. One plausible scenario is that the large defects in the OD developed first in the oxygen-contaminated surface region and that as the wall thickness was reduced, the cracks penetrated an ever greater fraction of the wall. The decrease in effective load –bearing cross section resulted in localized shear stresses sufficient to create a band of severe macroscopic deformation accompanied by grain rotation and elongation. Intersection of this band with the surface resulted in the development of a corresponding ID crack. The summary of the processing provided by ANL [1] and the notebook records at Century Tubes Inc. suggested a number of factors that could have resulted in the observed defects; these are discussed in the following.

The source material for Batch A tubing was the rectangular cross- section (63.5mmx190mm) as-extruded bar supplied by Teledyne Wag Chang Co. This material was used to produce the initial tube blank (27.9mm OD x 19.1mm ID x 200mm long) with the long direction parallel to the extrusion direction. The initial microstructure for Batch A was consequently very inhomogeneous and characterized by a mixture of small grains (20-60 microns),coarse equiaxed grains (100-200 microns) and banded regions of deformed (unrecrystallized) grains [7]. There is considerable evidence that Ti segregates strongly during ingot solidification and during extrusion at 1150ºC these regions become drawn out parallel to the extrusion direction and eventually give rise to the bands of Ti (CON) particles that characterize the subsequent cold worked and annealed microstructure.

During the processing of Batch A, the cold drawn tubing was encased in Ti foil and recrystallized at 1025ºC in a vacuum of ~7 x 10^{-5} torr. Furnace records show that because of the rapid heating rate employed, the vacuum quality often deteriorated into the 10^{-4} torr range as a result of out-gassing. The lack of control of the vacuum quality during heat-up is the most likely reason for the significant oxygen pick-up observed. Examination of the cleaning procedures used following each draw cycle suggested that the acrylic lubricant used was not completely removed during cleaning and was probably the source of the observed carbon pick-up.

The tube drawing cycle utilized in the production of Batch A is summarized in Table 1. A set of 10 draw cycles were used with intermediate recrystallization at 1025ºC for 1 hour; each draw cycle

consisting of 3 approximately equal passes. The reductions in area for the final 5 cycles were in the range 40-45%.and is it possible that these relatively high levels of work hardening coupled with oxygen pick-up could have led to the conditions which resulted in the development of the observed surface cracking. In addition, cycles 2-4 were drawn with a constant diameter mandrel so that the ID did not change ; this procedure necessitated a fairly heavy reeling operation to remove the tube from the mandrel prior to annealing and it is possible that this also contributed to the development of the surface cracks.

Table 1. Summary of drawing schedule used for Batch A tubing from US heat 832665 of V-4Cr-4Ti

Cycle No.	OD (ins)	ID (ins)	Wall (ins)	RA/Cycle (%)	Anneal No.
Tube blank	1.100	0.770	0.165		1
1	0.981	0.750	0.117	40.6	2
2	0.920	0.750	0.085	33.3	3
3	0.863	0.750	0.057	41.1	4
4	0.830	0.750	0.040	34.4	5
5	0.755	0.700	0.029	37.6	6
6	0.688	0.650	0.020	41.5	7
7	0.606	0.580	0.015	41.1	8
8	0.520	0.500	0.010	45.9	9
9	0.288	0.264	0.012	40.0	10
10	0.178	0.157	0.011	45.4	11

NIFS-HEAT-2

Before the second campaign at Century Tube was initiated, researchers at NIFS reported on the fabrication of a small quantity of pressurized creep tubing and some larger size tubing for tritium permeation studies using plate from the high purity NIFS-HEAT-2. A tube blank with a 25.0mm OD and 19mmID was machined from a cold-worked 26mm square section and initially recrystallized at 1000ºC. Tube reduction was carried using a 3-directional rolling process with intermediate annealing at 825ºC. This temperature was selected to minimize oxygen pick-up but is apparently sufficiently high to effect recrystallization with a final grain size of ~20 microns [4]. Creep tube fabrication was accomplished in 7 rolling passes, utilizing four anneals at 850ºC and one final anneal at 1000ºC resulting in a final grain size of 39 microns. The processing resulted in an increase in oxygen concentration of 200 wppm and an increase in carbon and nitrogen by 70 and 30 wppm respectively. Early problems with cracking were eliminated by a) lowering the heat treatment temperature of the initial plate to 1000ºC (finer grain size) and b) limiting the reduction in area per cycle to below 40%. The ID surface quality was improved by honing following gun drilling. The final creep tubing contained surface defects up to 20 microns deep and it was suggested that this cracking is related to the intersection of bands of Ti(CON) particles with the tube surfaces.

REVISED PROCEDURE FOR TUBING FABRICATION

Based upon the prior experience summarized above, a number of changes were introduced into the procedure for fabricating thin-wall tubing which were designed to decrease the magnitude of interstitial pick-up and to minimize the probability of generating the large surface defects which developed during the fabrication of Batch A of the US heat. The complete technical specification that is being followed in the current campaign to produce creep tubing from both the US and the NIFS heats of V-4Cr-4Ti is presented in the Appendix. The major changes introduced compared to the Batch A procedure are summarized below.

a) For the US heat, the initial as-extruded plate was cold worked 50-55% prior to recrystallizing at 1000ºC to give an average grain size of ~30 microns. Although this treatment did not improve chemical inhomogeneity or alter the distribution of Ti(CON) particles, the uniformity of the grain structure was greatly improved compared with Batch A. Gun drilling of tube blanks was followed by honing to a surface finish of 16 rms or better

b) A more rigorous cleaning operation was introduced after each draw cycle involving successive treatments in Alconox, acetone and ethyl alcohol followed by an acid cleaning.

c) Prior to annealing, the vacuum furnace was baked out at 100ºC above the annealing temperature to remove sources of contamination. Tubes were completely wrapped in tantalum foil and annealed in a vacuum of better than $2x10^{-5}$ torr; this vacuum was maintained during all out-gassing stages during heat-up. The first 4 annealing treatments were carried out at GA San Diego. Subsequently operations were transferred to a furnace that could accommodate up to 5ft tubing lengths at Bodycote Inc. where the vacuum was maintained in the 10^{-6} torr range.

d) To minimize stresses the drawing cycle was selected so that for the final 6 stages , the reductions in area did not exceed 30%. All draw cycles consisted of 3 approximately equal passes of mandrel draws using a series of mandrels of reducing diameter so that both the ID and OD were reduced in each cycle. Decreasing the reduction in area per cycle necessitated an increase in the number of annealing treatments with the corresponding risk of increase the amount of oxygen pick-up.

e) Archive samples for metallography and chemical analysis were removed after each draw and after each vacuum anneal.

INTERIM QUALITY ASSESSMENT

Tube Blanks

The starting material for the US Heat was a 28mm square cross-section measuring 230 mm long which had been cut from an extruded plate which had been cold rolled ~55%. A tube blank was machined measuring 25.7 mm OD and 15.7 mm ID. Ultrasonic testing and X-radiography failed to detect any defects in the tube blank. The source material for the NIFS-HEAT -2 was a 26mm thick plate, 28.6 mm wide and 200mm long from which a similar tube blank was machined. Ultrasonic testing of the NIFS tube blank indicated that several areas contained defects. Subsequent examination under low power stereo showed possible surface cracks 0.5-1.0mm long parallel to the rolling direction, several possible cracks at 45 degrees to the tube axis and several short 0.1-0.3mm circumferential defects. Nagasaka et. al also detected defects in the 26t plate material using ultrasonic methods and presented metallographic evidence for elongated cavities ranging up to 0.5mm long parallel to the extrusion direction [5].

Interstitial pick-up

Archive samples were removed after each draw cycle and after each annealing treatment. The results of chemical analysis for carbon oxygen and nitrogen up to the seventh drawing/eighth annealing cycle are shown in Table 3. At the end of the eighth anneal, the oxygen content of both heats has approximately doubled with very little change occurring in either nitrogen or carbon concentrations. With 5 more annealing treatments to complete the processing schedule, (Table 2), the increasing oxygen concentration is a concern. If the increase continues at the average rate of ~40 appm per cycle for the US Heat and ~30 wppm per cycle for the NIFS heat then the oxygen concentrations of the finished tubing could approach 850 and 530 wppm respectively. During the course of this study several anomalously high analyses were obtained for both oxygen and carbon and the origins of these results are difficult to pin down. It was established however that cutting specimens with a high speed saw produces surface oxidation and is a leading source of anomalously high oxygen analyses. This is probably not the only means of contaminating chemical analysis specimens and careful cutting

Table 2. Summary of drawing schedule for US heat 832665 (Batch B) and NIFS-HEAT-2 of V-4Cr-4Ti.

Cycle No.	OD (ins)	ID (ins)	Wall (ins)	RA/Cycle (%)	Anneal No.
Tube Blank	1.010	0.626	0.192		1
1	0.940	0.600	0.170	17.3	2
2	0.818	0.542	0.138	30.4	3
3	0.723	0.499	0.112	31.3	4
4	0.588	0.420	0.084	44.4	5
5	0.495	0.375	0.060	44.7	6
6	0.395	0.299	0.048	42.5	7
7	0.318	0.240	0.039	39.0	8
8	0.288	0.224	0.032	29.2	9
9	0.262	0.212	0.025	29.0	10
10	0.246	0.208	0.019	30.2	11
11	0.229	0.199	0.015	31.0	12
12	0.203	0.179	0.012	32.0	13
13	0.188	0.168	0.010	21.0	
SIZING	0.180	0.160	0.010	5.5	
				Final	

Table 3: Chemical analysis of tubing

Cycle No.	Wall (ins)	US HEAT			NIFS HEAT		
		C wppm	O wppm	N wppm	C wppm	O wppm	N wppm
Tube Blank	0.192	119	331	88	59	156	130
ANN 1	0.170	138	329	93	67	132	135
ANN 5	0.060	175	426	89	124	312	150
ANN 6	0.048	119	511	94			
ANN 7	0.039	155	494	84			
ANN 8	0.032	179	637	101	90	378	148

and cleaning procedures need to be rigorously followed to avoid contamination with oxygen or carbon.

Surface defects

At the end of the fifth drawing cycle numerous longitudinal surface defects were observed on the OD of the US heat tubing which at this stage had a wall thickness of 0.060 ins. One of the LT surfaces of the original plate was designated as the top surface (zero degrees), and the corresponding position on the tubing was tracked throughout the drawing sequence. The defects occurred in a band parallel to the drawing direction at a location 90 degrees from the original top surface of the plate. The defects appeared to consist of very shallow regions,1-2mm long, which had separated from the tube surface. Such defects are not uncommon in drawing tubes from BCC alloys and it is normal practice to remove them by local mechanical polishing before each draw. After the fifth draw the tube from the US heat was cut into 2 sections to fit into the annealing furnace. The region containing the defects

was confined to one tube (Tube A) while the second tube appeared to be defect-free (Tube A1). Despite careful polishing to remove the defects, they continued to appear in Tube A after each subsequent draw. After the tenth draw, it was possible to cut a sample from a region containing OD surface defects and a cross-section is shown in Fig.2. Comparison with Fig.1 shows that the surface defects are very similar to the type of defect frequently encountered in Batch A tubing from the US heat. Since these defects develop at an early stage in the drawing/annealing sequence and at a particular circumferential location, they are probably related to some macroscopic feature of the initial plate microstructure such as regions of highly banded microstructure, internal porosity or inclusions.

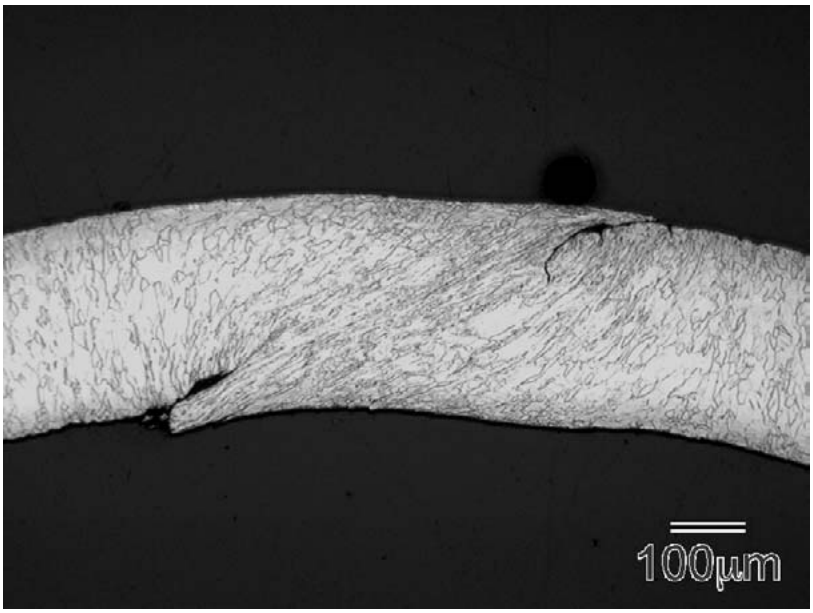

Figure 1. Surface defects in final tubing from US heat Batch A.

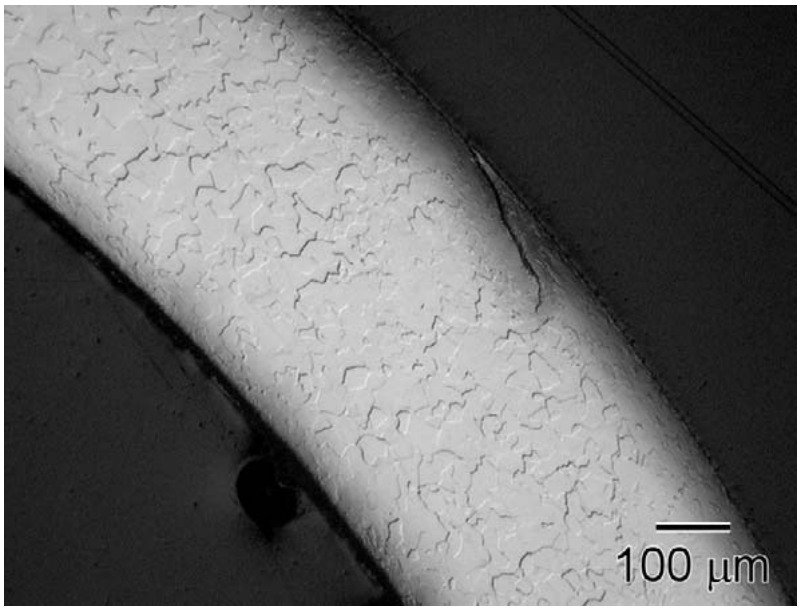

Figure 2. Surface defect in Tubing from US heat Batch B following the fifth drawing cycle.

Microstructure

Representative micrographs from both heats of tubing following the fourth draw cycle and fifth anneal are shown in Fig 3. The average grain size of the NIFS heat is very uniform with an average grain size of ~ 50 microns. The US heat contains a much higher fraction of small grains (5-10 microns) with an overall average size of ~ 28 microns. These differences are almost certainly related to the differences in initial interstitial content which is linked to the initial volume fraction and distribution of Ti(CON) particles. A cross section of the US heat following the third draw /fourth anneal is shown in Fig 4. This sample was stained during etching and at low magnification shows the macroscopic aspects of the deformation process during tube drawing. During etching, staining occurred along the bands of Ti(CON) particles revealing the significant macroscopic rotation of the grain structure which occurs as the outer surface is approached; the bands of particles apparently rotate with the deforming /rotating grains A similar phenomenon has been reported in the fabrication of NIFS heat tubing by 3-directional rolling and during cross-rolling of NIFS plate material [6]

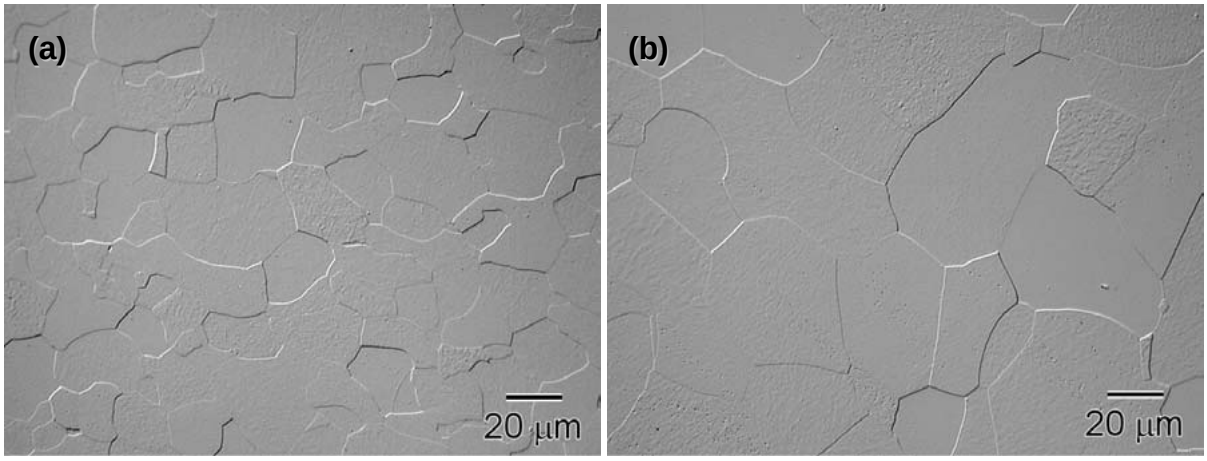

Figure 3. Grain structure of (a) US heat tubing (Batch B) and (b) NIFS heat tubing following the fifth annealing treatment.

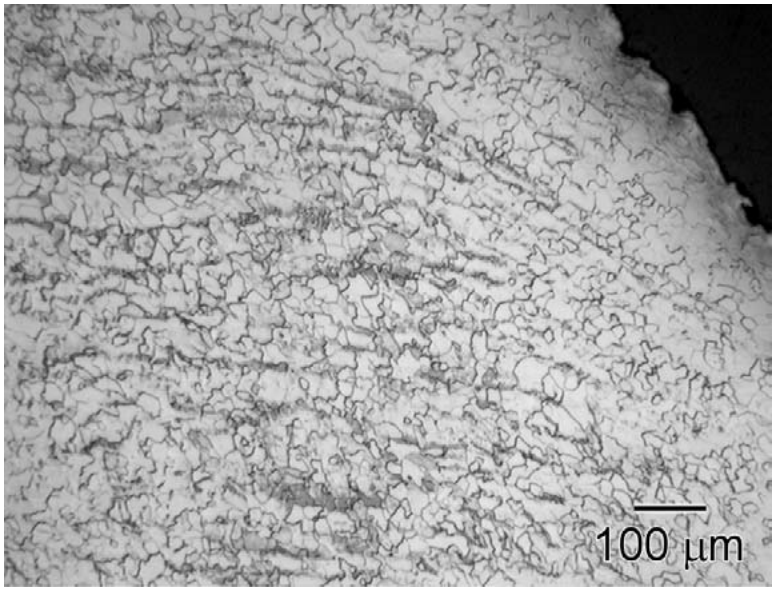

Figure 4. Optical micrograph with stain etch of the US heat (Batch B) following the 4th annealing treatment.

Future work

Fabrication of both heats will continue in accordance with the schedule shown in Table 2, paying close attention to the section of the US heat containing the visible defects and eliminating this section if necessary. Because of the development of different grain structures in the two heats it may be necessary to adjust the final heat treatment of the NIFS heat to reduce the grain size and ensure that there is a sufficient number of grains across the wall of the final creep tubing. A full evaluation of the finished tubing will be carried out including dimensional tolerance inspections, optical microscopy, TEM, chemical analysis, hardness, texture measurements and possibly ultrasonic and eddy current inspection.

REFERENCES

1. H. Tsai, M.C. Bilone, R.V. Strain, and D.L. Smith; Fusion Materials Semi-annual Progress Report DOE/ER-0310/23, December 1997, p149.
2. M.L. Grossbeck, R.J. Kurtz, L.T. Gibson and M.J. Gardner; Fusion Materials Semi-annual Report DOE/ER-0310/32, June 2002, p6.
3. H. Tsai, M.C. Billone, T.S. Bray and D.L. Smith; Fusion Materials Semi-annual Progress Report DOE/ER-0310/27,December 1999, p 65.
4. T. Nagaska, T. Muroga, T. Iikbo; “Development of Tubing Technique for High –Purity Low Activation Vanadium Alloys”, ANS Winter Meeting, Washington DC, Nov.2002, (to be published).
5. A.F. Rowcliffe and D.T. Hoelzer; Fusion Materials Semi-annual Progress Report DOE/ER-0310/25, December 1998, p42.
6. T. Nagasaka et. al, “Fabrication of High-Purity V-4Cr-4TiAlloy Products”; 2nd Workshop on the Development of Low Activation Vanadium Alloys for Fusion, NIFS, March 2002.

APPENDIX

TECHNICAL SPECIFICATION FOR FABRICATION OF THIN-WALL V-4Cr-4Ti ALLOY TUBING

TABLE OF CONTENTS

1.0 BACKGROUND

A V-4Cr-4Ti alloy is being studied as a possible structural material for first wall and blanket applications in Li-cooled fusion energy systems. Oremet Wah Chang of Albany, Oregon (OWCA), have produced a 500-kg heat (OWCA Heat 832665), for the United States Department of Energy (DoE)-funded Fusion Materials Sciences Program and a 1200-kg heat (OWCA Heat 832864) for General Atomics (GA), San Diego, California. A 30-kg heat (NIFS-HEAT-1) and a 166-kg. heat (NIFS-HEAT-2) with lower oxygen and nitrogen contents have been produced in Japan for the National Institute for Fusion Sciences. Thin-walled tubing of these alloys is needed to fabricate pressurized tube specimens for making creep property measurements in vacuum, liquid lithium, and neutron irradiation environments.

2.0 GENERAL INFORMATION

This specification establishes the requirements for the fabrication and heat treatment of thin-wall tubing to be used in the fabrication of specimens for irradiation creep experiments for the DoE Fusion Materials Sciences Program. Any additions or deletions to this specification shall be specified in applicable Oak Ridge National Laboratory (ORNL) service requests, memoranda, and/or drawings, and/or ORNL purchase orders/attachments. Should any conflicts develop between this specification and other technical documents referenced for the procurements or services indicated herein, this specification shall control. All such conflicts shall be resolved with the assigned ORNL representative before implementation. Any deviations to this specification by ORNL service organizations and/or outside contractors performing processes identified herein shall not be initiated without approval in writing by the assigned ORNL representative.

3.0 FABRICATION REQUIREMENTS

3.1 DEFINITION OF RESPONSIBILITIES

The assigned ORNL representative shall provide the raw material stock for fabricating the tubing. and provide certification of the chemistry of the raw material stock and any available fabrication history relative to same.

The assigned ORNL representative shall be responsible for the oversight of all processing steps in the fabrication of the tubing including characterization and preparation of the raw material stock, machining and dimensioning of the starting material (tube blank) for the initial tube fabrication, and fabrication, heat treatment, and dimensioning of the tubing .The ORNL representative shall also be responsible for the oversight of the characterization of the tubing at the designated hold points during processing and shall identify those ORNL service organizations or outside contractors who will be assigned to perform the characterization.

.

3.2 FABRICATION PROCEDURES

The specific procedures and requirements for the processing of tubing covered under this specification are defined in Section 5.0

3.3 MATERIAL CONTAMINATION PRECAUTIONS

The organizations identified herein for performing the various process steps in the fabrication of the tubing shall use necessary precautions to prevent exposure of the tubing material, during any process step, to any of the following:

The material shall not be exposed to any chlorine- or sulfur-bearing liquid, vapor, or grease during processing unless deemed specifically required for successful tubing fabrication, and which is known or can be shown to be removable by the cleaning processes designated herein prior to exposure to elevated temperatures (i.e. vacuum annealing or vacuum bakeout). The chemical nature of such required liquids, vapors, and/or greases with respect to the specific chemical species indicated herein shall be identified by the outside contractor prior to performing the work, and their specific use shall require approval by the assigned ORNL representative.

Except during tube drawing, expansion, and reduction (and mandrel removal) operations, the material shall not be allowed to come in contact with any metallic or non-metallic surface which may allow foreign particles of same to become embedded in its surface.

4.0 QUALITY ASSURANCE PROCEDURES

4.1 INSPECTION RIGHTS

The assigned ORNL representative shall have the right, during the working hours of the organization or outside contractor performing the work element, to witness inspections, perform product inspections, witness work operations in progress, and review quality documentation and records pertaining to the work indicated herein.

4.2 NOTIFICATION POINTS

Notification points shall be as a minimum the start of all processes designated in Section 5.0 Each notification point shall be witnessed at the option of the assigned ORNL representative who will be given two (2) working days advance notice. The outside contractor performing the work element shall not be required to hold up work once proper notification has been received by the assigned ORNL representative.

4.3 SAMPLING AND HOLD POINTS

At the end of each annealing cycle samples of tubing, to be specified by the ORNL representative, will be removed and placed in an archive. Samples will also be removed for chemical analysis and metallographic examination at ORNL. At the discretion of the ORNL representative, a hold time may be imposed until the results of chemical and microstructural analysis have been evaluated.

4.4 RECORDS MAINTENANCE

Outside contractors performing any of the work elements indicated herein shall submit inspection documentation, time-temperature and time-vacuum furnace charts, and other operations documentation and reports for inspection by the ORNL representative

5.0 FABRICATION PROCEDURES

5.1 CHARACTERIZATION OF THE RAW MATERIAL STOCK

The raw material stock to be used for fabrication of the tubing will be sections of cold–rolled plate measuring approximately 1.1 inches square and approximately 9 inches long. ORNL will provide material for three (3) sections of the US heat no.832665 and one (1) section of the Japanese heat NIFS-HEAT-2. The initial plate material will be characterized at ORNL in terms of optical microstructure, hardness and chemical analysis

5.2. MANUFACTURE OF TUBE BLANKS

The raw material stock shall be prepared for fabrication into material suitable for tubing (tube blank) as follows:

1) The raw material stock for the tubing shall be initially shaped and final machined using conventional machining methods to produce a tube blank (thick-walled tube) of dimensions suitable for processing into tubing of the required outside diameter (O.D.) and wall thickness. The method of machining and dimensions (O.D., wall thickness, and length) of the tube blank shall be agreed upon by the assigned ORNL representative and the vendor contracted to perform the processing of the tubing,. After machining, the finished tube blank shall be measured to record all physical dimensions and to determine its conformance to the specified dimensions. All measurements of these physical dimensions shall be documented. The finished tube blank shall be degreased in a solvent suitable

for removing visible traces of cutting debris and lubricants, and placed in a clean, dry, appropriately identified plastic bag.

2) The tube blank shall be cleaned in accordance with the procedure described in Section 5.3 and then annealed in accordance with the procedure described in Section 5.4 .

5.3 CLEANING TUBE BLANKS AND DRAWN TUBING

The starting material for fabrication of the tubing (tube blank) and subsequent as-fabricated tubing shall be cleaned prior to tube fabrication processes (drawing/expansion/reduction). Cleaning of the finished tube blank and as-fabricated tubing shall consist of solvent pre-cleaning, cleaning in a series of aqueous and solvent baths, and acid cleaning/etching (pickling), and shall be performed as follows:

5.3.1 SOLVENT CLEANING

The raw material stock for fabrication of tubing and as-fabricated tubing shall be solvent cleaned as follows:

1) Pre-clean the outer surfaces of the material to remove visual traces of any machining oils, marking ink, machining debris, etc., using a bristle brush or cloth and any suitable water-based or organic solvent cleaner (acetone, alcohol, etc.). Pre-clean the inner surfaces of the material to remove visual traces of any machining oils, machining debris, etc. by pulling or pushing multiple clean white solvent-soaked cotton or linen cloths through the internal bore of the material.

2) Clean external and internal surfaces of the material by immersion for a minimum of 5 minutes in each of the following series of solvent baths to remove all residues. Air dry material by placing on laboratory tissue (Kimwipes or equivalent) after each cleaning step. Verify removal of residues by surface wiping with a clean laboratory tissue moistened with ethyl alcohol.

   a) Bath 1 – Aqueous commercial cleaner (at >120ºF) [Alconox]

   b) Bath 2 - acetone (room temperature)

   c) Bath 3 - ethyl alcohol (room temperature)

3) If material has been saw cut (bandsaw, abrasive wheel, etc.), and saw-cut surfaces contain burrs, remove burrs by abrasive grinding saw-cut edges with #240 grit SiC paper (new).

4) If material has been electric discharge machined, abrasive grind machined surfaces with 600 grit SiC paper (new) to remove any discoloration and all evidence (by visual exam using 10X magnifier) of any brass residue from possible electrode interaction during discharge machining. Grind off a minimum of 0.0002 in. of surface material.

5) Wipe ground surfaces of material with ethyl alcohol-moistened tissue to remove all visual evidence of surface grinding debris. For tubular product forms, clean I.D. of tube by pulling or pushing ethyl alcohol-moistened cotton or linen cloth through tube to remove all visual evidence of surface grinding debris. Ultrasonically clean material in ethyl alcohol at room temperature. Air dry material on laboratory tissue (Kimwipes or equivalent). Handle cleaned material only with clean un-powdered rubber gloves or clean cotton or linen gloves.

6) Unless material is to proceed immediately through another process, e.g., pickling, annealing, etc., wrap material in laboratory tissue (Kimwipes or

equivalent) and place in a clean plastic bag appropriately identified as to sample identification, alloy designation, and material condition.

5.3.2 ACID CLEANING (PICKLING)

As soon as practical after solvent cleaning, all materials shall be acid cleaned as follows

1) Acid* clean/etch (pickle) material (maximum removal of 0.0005 in. of thickness) by immersion with agitation in a room temperature acid solution of 50 vol% deionized water - 30 vol% nitric acid - 20 vol% hydrofluoric acid for 30 seconds, followed by multiple rinses in deionized water at room temperature. Handle material with plastic tongs or by hand with clean un-powdered rubber gloves.

2) Wipe cleaned/etched and water-rinsed surfaces of material while still wet with deionized water-moistened cotton or linen cloth to remove all visual evidence of residue from acid cleaning/etching. For tubular product forms, clean I.D. of tube while still wet by pulling or pushing deionized water-moistened cotton or linen cloth through tube to remove all visual evidence of residue. For electric discharge machined materials remove all evidence of brass residue from prior machining (verify by visual exam using 10X magnifier). Ultrasonically clean material in ethyl alcohol at room temperature. Air dry material on laboratory tissue (Kimwipes or equivalent). Use clean un-powdered rubber gloves or clean cotton or linen gloves during etching/cleaning/wiping/handling of material. For electric discharge machined materials, repeat cleaning/etching/ rinsing/wiping procedure one additional time if visual evidence of brass residue persists. If repeat procedure is unsuccessful, hold at this point for review by the assigned ORNL representative.

3) Unless material is to proceed immediately through another process, e.g., vacuum annealing, etc., wrap fully-rinsed and dried material in laboratory tissue (Kimwipes or equivalent) and place in a clean plastic bag appropriately identified as to sample identification, alloy designation, and material condition.

**Caution: The acid etchant will generate some heat during its exposure to the material, and may cause severe burns from contact with unprotected tissue. A face shield and acid-resistant gloves should therefore be used at all times during handling of the acid and acid container(s).*

5.4 HEAT TREATMENT OF THE TUBE BLANK AND DRAWN TUBING

As soon as possible after cleaning as described above ,vacuum annealing should be carried out as follows:

1) Bake out vacuum furnace at a temperature at least 100ºC higher than the specified annealing temperature [see 4) below], and not more than 24 hours prior to the anneal.
2) Prior to annealing, wrap or shroud the material in a clean tantalum foil blanket such that no line of sight exists between the components of the vacuum furnace and any surface of the material to be annealed. Tantalum foil which has been previously used to anneal material in accordance with Section 5.4 or which has been baked out during or in a manner similar to the furnace bakeout step indicated in 1) above shall be acceptable. Support the material in the furnace to prevent distortion, or bowing. The material may be placed in the furnace either horizontally, vertically, or at an angle as long as proper support is provided.

3) Vacuum anneal the material using the following procedure:

a) Heat the material from room temperature to 525ºC at a rate commensurate with maintaining a vacuum of 2 x 10^{-5} torr or better. Hold at 525 ± 10ºC for 1 hour.

b) Heat the material from 525ºC to 1000ºC in a vacuum of 2 x 10^{-5} torr or better, and at a rate of 400ºC - 600ºC/hour. Hold at 1000 ± 10ºC for 1 hour.

c) Cool material to 50ºC in a vacuum of 2 x 10^{-5} torr or better, and at a rate of >1000ºC/hour (nominal). Do not remove material until temperature of material is <50ºC. Use clean cotton or linen gloves during handling.

d) Monitor the temperature and temperature uniformity of the material using a minimum of two (2) thermocouples (e.g., Type K, with Inconel 600 sheath) attached directly to the material or inserted into the tantalum-wrapped material/ package. If the uniformity of the furnace has been previously established and accepted by the assigned ORNL representative, only one (1) thermocouple attached to the material or inserted into the Ta-wrapped material/package is required.

5) Record temperature and vacuum level readings in a continuous fashion, or manually every 10 minutes, during heat up, elevated-temperature holds, and cool down of the material.

6) After removal of the wrapped material from the vacuum furnace, unwrap material. Wrap material in laboratory tissue (Kimwipes or equivalent) and place in a clean plastic bag appropriately identified as to sample identification, alloy designation, and material condition. Place tantalum foil in a clean plastic bag and provide to the assigned ORNL representative.

5.5 TUBING FABRICATION (TUBE DRAWING/EXPANSION/REDUCTION)

Tube blank material prepared in accordance with Sections 5.1 through 5.5 shall be fabricated into tubing of the required outside diameter (O.D.) and wall thickness. The dimensions of the tube blank required to produce the required finished tubing dimensions shall be agreed upon by the assigned ORNL representative and the vendor contracted to perform the fabrication of the tubing. The tube blank and finished tubing dimensions shall be specified in the ORNL purchase order for the processing of the tubing. Fabrication of the tubing shall be performed as follows:

1) The finished, cleaned, and annealed tube blank shall be fabricated into tubing by drawing at room temperature in accordance with the dimensions (O.D. and wall thickness) specified in the ORNL purchase order for the processing of the tubing. A step-by-step fabrication schedule to be followed in drawing the tubing, including die and mandrel sizes for each draw pass, shall be provided to the assigned ORNL representative by the outside contractor processing the tubing prior to the initiation of processing. The tolerance on the tube O.D. shall be ± 0.001 in. and the tolerance on the tube I.D. shall be ± 0.001ins.Finished tube ovality shall not exceed 0.002ins and eccentricity shall not exceed 0.0005ins. The fabrication of the finished tubing will require several draw cycles, of several draw passes each, and several intermediate cleanings/anneals.

2) Prior to initial drawing, one end of the tube blank shall be swaged (pointed) to facilitate entry into the drawing die. The swaged length (point) shall be minimized in order to facilitate the fabrication of the longest length of tubing possible, but shall not be made so short as to compromise the fabrication of the tubing itself. The tube blank shall be reduced through successively smaller dies until both its O.D. and wall thickness reach the final tube dimensions specified, or

reduced through successively smaller dies until its wall thickness reaches the specified wall thickness, and then expanded or reduced in diameter to the specified O.D. The reduction in area for each drawing pass shall be limited to 15 ± 2%. The total reduction for the first draw cycle shall be limited to 30 ± 5%; the total reductions for succeeding draw cycles up until the last two draw cycles shall not exceed 45%; and the total reductions for the last two draw cycles shall be limited to 30 ± 5%. The outside diameter, wall thickness, length, and hardness (near trailing end) of the tubing shall be measured and recorded after each draw (pass) to assess the progress of the processing. A report of the tubing dimensions and hardness values recorded after each pass shall be provided with the finished tubing.

3) After each draw cycle, and prior to cleaning/annealing, two (2) cross-sections (each ~1/4 in. in length) shall be taken from the trailing end (non-pointed end) of the tubing) using conventional cutting methods (abrasive wheel, bandsaw, EDM, etc). After cutting, the tubing sections shall be degreased in a solvent suitable for removing visible traces of machining debris and lubricants, and placed in a clean, dry, plastic bag appropriately identified as to sample identification, alloy designation, and material condition. The tube blank sections shall be provided to the assigned ORNL representative.

4) The remaining tubing shall be cleaned and vacuum annealed in accordance with the procedures described in Sections 5.3 and 5.4.

5) The step-by-step fabrication schedule may be necessarily changed or altered by the tube processing vendor during the actual fabrication process depending on the actual final dimensions of the starting tube blank, possible failure of the material to achieve the specified deformation levels, etc. Such changes shall require approval in writing by the ORNL representative prior to initiation.

6.0 PACKAGING AND SHIPMENT

6.1 IDENTIFICATION AND MARKING

The finished tubing shall be marked with the supplier's identification, lot number, nominal thickness or diameter and purchase order number. Markings shall be made on one surface of each product piece. Characters shall be of such size as to be clearly legible, and shall be applied using a suitable marking fluid capable of being removed with conventional cleaning solutions without excessive rubbing. The markings or their method of removal shall have no deleterious effect on the product or its intended performance, and shall be sufficiently stable to withstand normal handling.

6.2 PACKAGING AND PACKAGE MARKING

The product shall be prepared for shipment in accordance with commercial practice and in compliance with applicable rules and regulations pertaining to the handling, packaging, and transportation of the product to ensure carrier acceptance and safe delivery. Each piece of product form shall be individually wrapped in a protective material to preclude exposure to atmospheric conditions and/or improper handling which could inadvertently damage the material. Packaging shall conform to carrier rules and regulations applicable to the mode of transportation utilized for shipment of the product.

7.0 ACKNOWLEDGEMENT

The supplier shall specifically mention this specification number and revision letter in all quotations and when acknowledging contracts or purchase orders.

2.0 CERAMIC COMPOSITE MATERIALS

THERMAL DIFFUSIVITY/CONDUCTIVITY OF IRRADIATED SYLRAMIC™ 2D-SIC$_F$/SIC COMPOSITE

G. E. Youngblood, D. J. Senor and R. H. Jones (Pacific Northwest National Laboratory)*

OBJECTIVE

The primary objective of this task is to assess the thermal conduction properties of SiC$_f$/SiC composites made from SiC fibers (with various SiC-type matrices, fiber coatings and architectures) before and after irradiation, and to develop analytic models that describe the transverse and in-plane thermal conductivity of these composites as a function of constituent properties and geometry as well as temperature and dose.

SUMMARY

A 2D-SiC$_f$/SiC composite was made by Hypertherm with an ICVI-SiC matrix and with multilayer C/SiC coatings on high thermal conductivity Sylramic™ fibers woven into 5HS fabric layers. Thermal diffusivity measurements were made on representative samples of this Sylramic™ composite before and after irradiations in the HFIR reactor as part of the JUPITER 14J test series. The irradiations took place at about 290 and 800°C to equivalent doses of 4.2 and 7.0 dpa-SiC, respectively. The ratios of the transverse thermal conductivity after-to-before irradiation (K_{irr}/K_o) determined at the irradiation temperature were estimated from thermal diffusivity measurements to be about 0.12 and 0.37 at 290 and 800°C, respectively. However, the measured thermal diffusivity values of the unirradiated Sylramic™ composite with multilayer C/SiC fiber coatings were about 40% less than values predicted by the H2L model for this composite. This observation could be explained if the net interface conductance of the C/SiC multilayer was less than 0.1 of the interface conductance of a single layer PyC fiber coating.

PROGRESS AND STATUS

Introduction

The purpose of this study was to examine the effects of a C/SiC multilayer fiber coating on the thermal conduction properties of a SiC$_f$/SiC composite reinforced with a high conductivity SiC fiber. In particular, the H2L thermal conductivity model predicts that a composite with low fiber-matrix (f/m) interface conductance would thermally decouple the fiber from the matrix [1]. If the C/SiC multilayer interface, in fact, exhibits a low net interface conductance, the expected beneficial influence of using a fiber with a high thermal conductivity to achieve a composite with an overall high transverse thermal conductivity may be nullified.

It is noted that SiC$_f$/SiC composites with a multilayer interphase have exhibited improved toughness [2] and oxidation resistance [3] compared to composites similarly made except with a single layer PyC interphase. Furthermore, Snead and Lara-Curzio showed that for a set of similar SiC$_f$/SiC composites made with Hi-Nicalon™ fabric, but with a conventional single layer carbon, a pseudo-porous SiC, or a multilayer C/SiC interphase, the composite with the multilayer C/SiC interphase exhibited the least degradation (8-20%) in the ultimate bend stress after irradiation to 1.1 dpa at 385°C [4]. Thus, the multilayer C/SiC fiber coatings are expected in some cases to promote improved mechanical performance in both unirradiated and irradiated SiC$_f$/SiC composite.

In this companion report to [1], the H2L model is used to critically assess the overall transverse thermal conductivity before and after irradiation for a 2D-SiC$_f$/SiC composite made with a high thermal conductivity fabric and a C/SiC multilayer fiber coating. The examined composite was made by

* Pacific Northwest National Laboratory (PNNL) is operated for the U.S. Department of Energy by Battelle Memorial Institute under contract DE-AC06-76RLO-1830.

Hypertherm using a Sylramic™ fabric. The primary differences in this composite compared to the Hi-Nicalon™ composites discussed in the previous report were replacing the Hi-Nicalon™ fabric and its single layer PyC fiber coating with Sylramic™ fabric and its multilayer C/SiC fiber coating. Otherwise, the Sylramic™ and Hi-Nicalon™ composites had a similar ICVI-SiC matrix and similar bulk density values.

Composite Samples

The Sylramic™ fiber was prepared from a polymer-derived Si-C-O fiber by Dow Corning Corporation and had the following nominal properties: mean fiber diameter 10 μm, density 3.0-3.1 g/cc, tensile strength 3.2 GPa, tensile modulus 380 GPa, thermal conductivity 40-46 W/mK, crystallite grain size 100 nm, and thermal stability to 1600°C [5]. By using several processing steps including a high temperature sinter, a crystalline fiber results with essentially stoichiometric SiC (95% wt.), TiB_2 grains (3% wt.) at triple points and small amounts of B_4C (1% wt.) and BN. The high density and high degree of crystallinity in the fiber promote a high elastic modulus and thermal conductivity. Because the diameter is small, this fiber can be readily woven into 2D fabrics, even though the modulus of the Sylramic™ fiber is quite high.

The Sylramic™ composite, made by Hypertherm with a x4 C/SiC multilayer fiber coating applied by CVD prior to matrix infiltration by ICVI, was provided by G. Newsome (KAPL) as a 0.125" x 2.0" x 4.0" plate. The Sylramic™ fabric had 800 filaments/tow and was five-harness satin weave (5HS). In the composite plate, thirteen plies were stacked with a 0-90 lay-up. Prior to cutting out individual samples, the plate was diamond milled on one surface to a constant 2.26-mm thickness. Four thermal diffusivity samples (TS1-4, 9.3 mm dia. X 2.26 mm thick) and 21 flexural bars (30 x 6.0 x 2.26 mm) were diamond cored or sawed from the milled plate. The bulk density values, determined by simple weighing and measuring of the sample dimensions, were in a similar range as the composites made with Hi-Nicalon™ fabric (2.44-2.60 g/cc). These bulk density values suggest that the macroporosity values were in the 15-20% range for the Sylramic™ composites, whereas the Hi-Nicalon™ composites had macroporosity values in the 7-13% range.

Irradiation and Test Conditions

Thermal diffusivity measurements were made simultaneously on several sample discs at various temperature steps in air from RT to 400°C before and after irradiation using the "low temperature" laser flash diffusivity system as described previously [1]. By plotting the reciprocal of the measured thermal diffusivity values versus temperature in degrees K, the resulting linear fit was used to extend diffusivity values to higher temperatures for analysis. The Sylramic™ composite disc samples were irradiated in the HFIR reactor at ORNL as part of the JUPITER 14J test series (TS1-2 at 290 ± 20°C, 4.2 dpa-SiC and TS3-4 at 800 ± 5°C, 7.0 dpa-SiC). All diffusivity measurements were made in air, but no annealing treatments were given to these Sylramic™ composites (as were carried out for the Hi-Nicalon™ composites).

Results and Discussion

In Figure 1, the thermal diffusivity values as a function of temperature for the Sylramic™ ICVI-SiC composite with a multilayer C/SiC interface are presented for various conditions. The conditions were: [1] as-received sample TS4 with a bulk density of 2.60 g/cc, [2] samples TS3 and TS4 irradiated at 800°C to an equivalent dose of 7.0 dpa-SiC, and [3] samples TS1 and TS2 irradiated at 290°C to an equivalent dose of 4.2 dpa-SiC. Although not accurately determined by simple dimensional measurements, a volume change of the disc samples irradiated at 290°C and 800°C appeared to exhibit roughly a 2.5-4.0% and 1.5-2.5% expansion, respectively.

In general, the unirradiated samples with higher bulk density values exhibited higher thermal diffusivity values. Since sample TS4 had approximately the same bulk density (2.60 g/cc) as the previously tested

Hi-Nicalon™ samples with the “thin” interface, the thermal diffusivity data for this specific sample with a high thermal conductivity Sylramic™ fiber component was used for detailed analysis. The measured thermal diffusivity of this sample was about 0.076 cm^2/s at RT and decreased continuously with increasing temperature to about 0.04 cm^2/s at 500°C. The thermal diffusivity curve for sample TS4 approximately matches the curve determined for the Hi-Nicalon™ composite with a “thin” PyC interphase [1]. The corresponding transverse thermal conductivity values also approximately match the Hi-Nicalon composite values (14 and 9 W/mK at RT and 1000°C, respectively).

Assuming that the ICVI-SiC matrix in the Sylramic™ composite has the same thermal conductivity values as determined for the ICVI-SiC matrix in the Hi-Nicalon™ composite, the H2L model predicts thermal diffusivity values that should be about 40% higher than the observed values. This is the case even if the somewhat higher porosity factors in the Sylramic™ composite are considered. This observation can be explained if the net interface conductance for the x4 C/SiC multilayer fiber coating is less than 0.1 of the value determined for the single layer PyC fiber coating. At this time, microstructural analysis has not

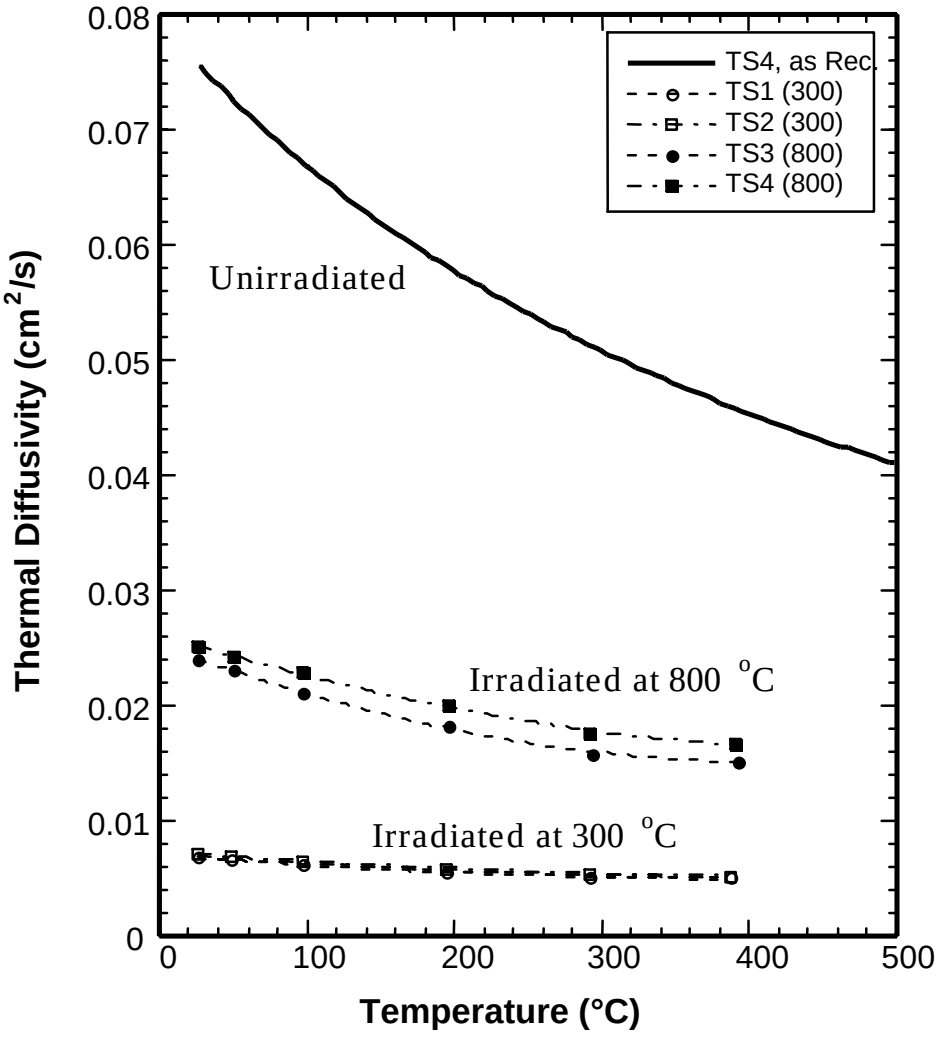

Figure 1. The measured thermal diffusivity values for representative Sylramic™ fiber-reinforced 2D-SiC_f/SiC composite samples made with multilayer C/SiC interphase before and after irradiation at 290°C (4.2 dpa-SiC) and 800°C (7.0 dpa-SiC).

been carried out on these Sylramic™ composites. Nevertheless, further analysis of this potential thermal conduction problem for other SiC_f/SiC composites made with multilayer fiber coatings is warranted.

After irradiation beyond saturation doses, the thermal diffusivity of the Sylramic™ composite was severely degraded as expected (Figure 1). Similar to the Hi-Nicalon™ composite case, the degradation was significantly larger for the irradiations at 290°C compared to those at 800°C. If it is assumed that the density and heat capacity values weren't significantly affected by the irradiation, then the ratio K_{effi}/K_{effo} is approximately 0.12 or 0.37 at 290 and 800°C, respectively. Again, the general trend that this ratio tends to gradually increase with increasing temperature for irradiated SiC_f/SiC composites and monolithic SiC is observed [6].

Further analysis of these data is not warranted until microstructural examinations have been carried out. Also, at this point the potential negative influence on the irradiation performance of the Sylramic™ composite due to the enhanced helium production in the Sylramic™ fibers with substantial boron content has not been considered.

FUTURE WORK

Detailed dimensional analysis will be performed on bar samples of the Sylramic™ composite irradiated in the 14J experiment. Also, if warranted flexural stress-strain measurements and microstructural examinations will be made and correlated with the thermal property results.

REFERENCES

[1] G. E. Youngblood, D. J. Senor and R. H. Jones, "Thermal diffusivity/conductivity of irradiated Hi-Nicalon™ 2D-SiC_f/SiC composite," in this Fusion Materials Semiannual Progress Report.

[2] Sebastien Bertrand, Rene Pailler and Jacques Lamon, "Influence of strong fiber/coating interfaces on the mechanical behavior and lifetime of Hi-Nicalon/(PyC/SiC)n/SiC minicomposites," J. Amer. Ceram. Soc. 84(4), 787-794 (2001).

[3] Y. Katoh, K. Hironaka, T. Hinoki and A. Kohyama, "Environmental effects of interfacial integrity of advanced SiC fiber-reinforced SiC matrix composites," Ceram. Eng. and Sci. Proc. 22 (4), 2001.

[4] L. L. Snead and E. Lara-Curzio, "Interphase integrity of neutron irradiated silicon carbide composites," p. 100 in Fusion Materials Semiannual Progress Report for period ending December 31, 1998 (DOE/ER-0313/25).

[5] R. E. Jones, J. Rabe and D. Petrak, "Sylramic™ SiC fibers for CMC reinforcement," p. 22 in the Proceedings of the 3rd IEA SiC/SiC Workshop, January 29-30, 1999, Cocoa Beach, FL.

[6] D. J. Senor, G. E. Youngblood, C. E. Moore, D. J. Trimble, G. A. Newsome and J. J. Woods, "Effects of neutron irradiation on thermal conductivity of SiC-based composites and monolithic ceramics," Fusion Technology 30(3), 943-955 (1996).

THERMAL DIFFUSIVITY/CONDUCTIVITY OF IRRADIATED MONOLITHIC CVD-SIC -
G. E. Youngblood, D. J. Senor and R. H. Jones (Pacific Northwest National Laboratory)*

OBJECTIVE

The primary objective of this task is to assess the thermal conduction properties of SiC before and after irradiation and after various high temperature heat treatments. Analytic models will be used to describe the fundamental behavior of the thermal conduction process in SiC as a function of microstructural properties as well as temperature and radiation dose.

SUMMARY

Several thermal diffusivity disc samples of high purity CVD-SiC were neutron-irradiated to equivalent doses of about 5-8 dpa-SiC at temperatures from 252 up to 800°C. For this temperature range, the degradation in the thermal diffusivity ranged from about 95% down to 89%, respectively. The reciprocal thermal diffusivity method was used to estimate the phonon mean free paths and defect concentrations before and after the irradiations for these materials. Even though the CVD-SiC material is an excellent monitor of certain neutron irradiation effects, the degradation in the thermal diffusivity (conductivity) appears to be more than a factor of two greater than predicted by recent theoretical model simulations.

PROGRESS AND STATUS

Introduction

A SiC material is exceptionally useful for monitoring some engineering aspects of neutron irradiation. For instance, in 1972 Price developed a method whereby SiC could be used to estimate the temperature inside a capsule during irradiation in a nuclear reactor by monitoring the recovery of its volume swelling after a series of high temperature anneals [1]. In 1995, a similar but more sensitive method for estimating the capsule irradiation temperature was examined at PNNL where the thermal diffusivity recovery rather than the volume swelling recovery was monitored also after a series of high temperature anneals [2]. This was possible because in SiC the thermal conductivity is determined by lattice or phonon conductivity, and in high purity SiC the phonon conductivity is extremely sensitive to the number of lattice imperfections. In high purity SiC neutron-irradiated at moderate temperatures (200-800°C), the lattice imperfections consist primarily of radiation-induced point defects (vacancies and interstitials). By measuring the temperature dependence of the thermal conductivity (or diffusivity) for the irradiated SiC, the phonon mean free path can be estimated and the spacing (or concentration) of the radiation-induced point defects deduced.

Originally, the analysis method developed at PNNL was used to estimate the phonon mean free path for high purity and Be-doped SiC by examining the temperature dependence of the reciprocal thermal diffusivity [3]. In this report, the reciprocal thermal diffusivity method is used to estimate the phonon mean free path for high purity Morton CVD-SiC before and after neutron irradiation at various temperatures. Then, from the calculated phonon mean free paths the radiation point defect concentrations are estimated and compared to some recent theoretical predictions by Li, et al [4].

CVD-SiC Material

The monolithic chemical vapor deposited (CVD) SiC material is a commercial product manufactured by Morton Advanced Materials (now Rohm and Haas) [5]. In the CVD process, methyltrichlorosilane (MTS)

* Pacific Northwest National Laboratory (PNNL) is operated for the U.S. Department of Energy by Battelle Memorial Institute under contract DE-AC06-76RLO-1830.

gas is decomposed onto a carbon substrate at about 1350°C. The CVD material is extremely pure, with typical impurity concentrations of less than 5 wppm. The crystal structure is cubic (3C polytype, commonly referred to as β-SiC) so provides isotropic characteristics. The grain size is between 5 and 10 μm in the plane parallel to the substrate, but the grains are elongated in the <111> growth direction perpendicular to the substrate. The material is homogeneous and typically free of microcracks or other large flaws, but atomic layer stacking faults on the {111} planes are common. There is no porosity in CVD-SiC, and the material is generally considered to be theoretically dense (approximately 3.21 g/cc). The material is stiff (elastic modulus 466 GPa), and has high chemical resistance, thermal conductivity and stability at high temperatures. Therefore, CVD-SiC makes an excellent reflective optics material or electronics substrate, and also an excellent reference material for analyzing neutron irradiation effects.

Reciprocal Thermal Diffusivity Method

The thermal conductivity (k) in SiC is determined by lattice or phonon conduction. An empirical approach, in analogy to the kinetic theory of gasses, relates k for an isotropic solid to the phonon mean free path (λ) via

$$k = 1/3VC_v\lambda \quad (1),$$

where V is the phonon group velocity and C_v is the specific heat at constant volume [6]. In turn, k also may be expressed in terms of the more easily measured thermal diffusivity of the material (α) as

$$k = \alpha\rho C_p \quad (2),$$

where C_p is the specific heat at constant pressure and ρ is the bulk density. By setting Eq. (1) = Eq. (2), the thermal diffusivity may be expressed as

$$\alpha = 1/3V\lambda \quad (3),$$

if the assumption that C_v is approximately equal to ρC_p (generally valid to within 10% up to the melting point of the material). Using α(T) for analysis rather than k(T) eliminates the complicating issue of considering the temperature dependence of C_v. Estimating λ then becomes a diffusion problem rather than an energy transport problem. For SiC, this is important since the temperature range of interest here covers 200°C <T<800°C and the Debye temperature (θ_D = 1080K) lies within this range [7]. The phonon group velocity, estimated from the speed at which vibrations propagate through an elastic material ($V = (E/\rho)^{1/2}$) is about 1.2 x 10^4 m/s for SiC and is only slightly temperature dependent. By inverting and expanding Eq. (3), the reciprocal thermal diffusivity is expressed as

$$1/\alpha = (3/V)\sum_i(1/\lambda_i) = (3/V)\{1/\lambda_o + 1/\lambda_d + 1/\lambda_p\} \quad (4),$$

where the subscripts o, d and p represent the phonon mean free paths associated with intrinsic defects, radiation-induced defects and phonon-phonon interactions, respectively. At higher temperatures ($T>\theta_D$), the phonon mean free paths for defects become temperature independent, and the temperature dependence of 1/α will be dominated by the temperature dependence of the phonon-phonon (Umklapp) interactions. Even at temperatures somewhat below θ_D, the temperature dependence of λ_o and λ_d can be considered temperature independent if the temperature dependence of λ_p is described by

$$\lambda_p = b/(T - T_o) \quad (5),$$

where b is a constant and $T_o = \theta_D/3$ = 360K for SiC. Substituting Eq. (5) into Eq. (4),

$$1/\alpha = (3/V)\{1/\lambda_o + 1/\lambda_d - T_o/b + T/b\} = A + B(T). \quad (6),$$

where $A = (3/V)\{1/\lambda_o + 1/\lambda_d - T_o/b\}$ (7a)

and $B = 3/Vb$ (7b)

If the distribution of the intrinsic and the radiation-induced point defects is assumed to be uniform, the cubic volume λ^3 surrounding each defect is given by a_o^3/NX where a_o is the lattice parameter for β-SiC (0.436 nm), N = 8 is the number of atoms in the unit cell defined by a_o, and X is the fractional concentration of point defects (intrinsic plus radiation-induced). Then the defect inverse mean free path ($1/\lambda$) can be calculated from Eqs. (7a) and (7b) by

$$1/\lambda = 1/\lambda_o + 1/\lambda_d = AV/3 + T_o/b \quad (8),$$

and the defect concentration (X) is

$$X = (1/\lambda)^3 a_o^3/N \quad (9)$$

Irradiation and Test Conditions

The thermal diffusivity of several unirradiated or irradiated CVD-SiC discs (9.5 mm dia. X 2.5 mm thick) was measured simultaneously in air as a function of temperature up to about 400°C by the laser flash method described previously [8]. Unirradiated samples on which the thermal diffusivity had already been measured were then irradiated in the HFIR reactor at ORNL as part of the JUPITER 11J-12J and 14J test series. The samples were irradiated in helium-filled capsules during seven HFIR-cycles at approximately constant, but different temperatures to doses well above saturation (for SiC saturation doses typically are <1 dpa-SiC). For doses above saturation, the SiC acquires a quasi-equilibrium concentration of radiation-induced defects, mostly vacancies and interstitials. After irradiation, the thermal diffusivity was remeasured on these same samples from RT to just below the irradiation temperature. The sample temperatures were held below the irradiation temperature to prevent defect annealing during the measurements.

In Table 1, the specific irradiation conditions for each sample are listed in order of increasing irradiation temperature. Temperature control during irradiation was more difficult for the lower temperatures, so the listed irradiation temperature is end-of-run temperature after seven cycles. The sample loading and irradiation cycle operation details are given in [9a-b].

Table 1. Irradiation conditions for CVD-SiC samples tested in JUPITER 11J or 14J.

Sample ID	Test	Eq. Dose (dpa-SiC)	Irrad. Temp.* (°C)	Est. $\Delta V/V_o$ (%)	α_{irr}/α_o ($\approx k_{irr}/k_o$)
M1	11J	7.9	252 ± 19	2.6	0.044
N5	14J	5.0	310 ± 20	2.5	0.050
N6	14J	5.1	310 ± 20	2.4	0.047
N7	14J	5.2	310 ± 20	2.5	0.046
M2	11J	7.1	355 ± 33	2.3	0.067
N3	14J	6.1	480 ± 20	2.2	0.062
N1	14J	6.8	800 ± 10	1.5	0.134
N2	14J	6.9	800 ± 10	1.5	0.113

*End-of-run temperature

Results and Discussion

In Table 1, the estimated relative volume changes (radiation-induced swelling, $\Delta V/V_o$) were determined from changes in the bulk density measurements made for each disc sample. The listed swelling estimates appear to be 20-30% higher than expected for each irradiation temperature. Nevertheless, the almost linear rate of swelling decrease with increasing irradiation temperature closely follows expected swelling behavior for SiC [10]. The dimensional measurements, carried out with a micrometer, were consistent but perhaps not very precise, which might explain the 20-30% discrepancy. Also, the irradiation temperatures monitored in the 300°C capsule tended to increase slightly (20-40°C) during each cycle [9a-b].

In Figure 1, the measured 1/α-data are graphically presented as a function of temperature (K) for each irradiated CVD-SiC sample listed in Table 1. For reference, the straight line fit to the average 1/α-data for unirradiated CVD-SiC is shown as a solid line near the bottom of the figure.

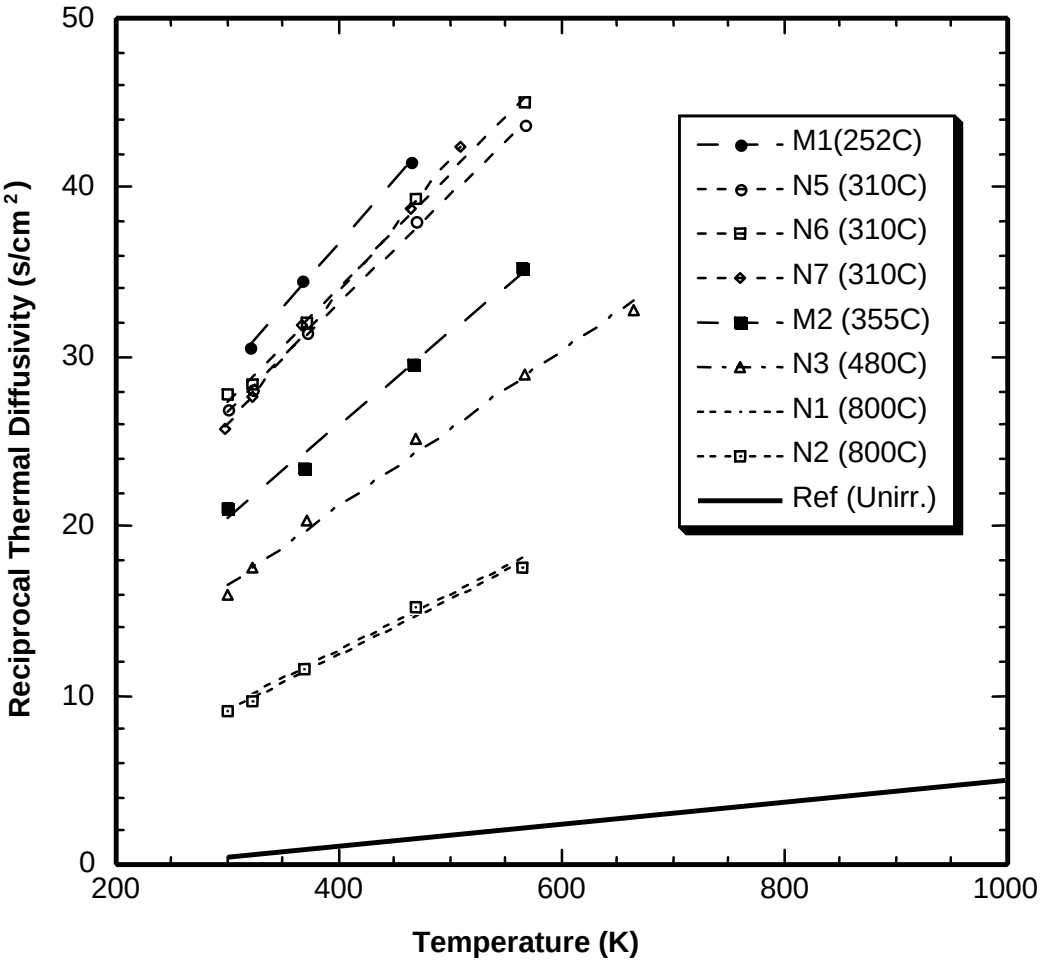

Figure 1. Comparison of the reciprocal thermal diffusivity values determined for several CVD-SiC samples irradiated at different temperatures (irradiation temperature shown in parenthesis) with reference values determined for unirradiated Morton™ CVD-SiC (solid line).

The solid reference line for CVD-SiC was calculated from the α(T)-curves measured before the irradiation for the six samples (N1-N7). The individual α(T)-curves for these unirradiated CVD-SiC samples exhibited characteristic ~1/T temperature dependence, but also a significant spread (±20%). Importantly, repeated measurements on the same sample typically reproduced α-values to ±5%. Apparently, the sample-to-sample variations were real and likely were caused by subtle differences in microstructure even though the sample discs were cut from the same plate. The ±20% spread in the α(T)-curves illustrates the importance of monitoring changes in diffusivity for the same sample before and after irradiation to properly assess changes in diffusivity due to radiation effects.

The intercepts A and slopes B, determined from a linear least squares fit to the 1/α-data for each sample according to Eq. (6) and shown as dashed lines in Figure 1, are listed in Table 2 along with their fit correlation factor R^2. Also listed are the λ- and X-values calculated by Eqs. (8) and (9), respectively.

Table 2. Phonon mean free path and point defect concentration calculations for CVD-SiC samples.

Sample ID	Irrad. Temp (°C)	A (s/cm^2)	B (s/cm^2K)	R^2	λ (nm)	X (appm)
M1	252 ± 19	6.497	0.0755	0.9993	0.74	25,300
N5	310 ± 20	7.624	0.0641	0.9986	0.81	19,200
N6	310 ± 20	7.257	0.0671	0.9957	0.80	20,500
N7	310 ± 20	2.743	0.0778	0.9984	0.81	19,300
M2	355 ± 33	4.016	0.0548	0.9948	1.05	8,900
N3	480 ± 20	2.827	0.0460	0.9931	1.29	4,800
N1	800 ± 10	-0.628	0.0332	0.9893	2.21	960
N2	800 ± 10	-0.745	0.0330	0.9937	2.25	920
Ref.	-	-0.824	0.0054	0.9986	22.2	0.9

The linear fits of the 1/α-data are exceptionally good with correlation coefficients near 0.99. The calculated λ-values decrease continuously from about 22 nm (~50 lattice constants) for the unirradiated reference CVD-SiC down to 0.74 nm (~2 lattice constants) for the sample irradiated at the lowest temperature (252°C). The calculated defect concentration for the reference sample is less than 1 appm, which is consistent with the manufacturer's value of <5 wppm impurities. The defect concentrations for the irradiated CVD-SiC samples decrease continuously from about 25,000 to 920 appm as the irradiation temperature increases from 252 to 800°C. The small concentration of intrinsic defects (<1 appm) in comparison to the extrinsic defect concentrations (>920 appm) illustrates why CVD-SiC makes an ideal irradiation damage monitor. Furthermore, these defect concentration estimates represent saturated values so should be relatively independent of dose.

In a theoretical study of the thermal properties of crystalline β-SiC, Li, et al, used a molecular dynamics simulation together with an empirical potential model to evaluate directly the heat capacity, thermal expansion and thermal conductivity for a perfect crystal, which were in excellent agreement with experimental data [4]. Then by introducing a single defect into the simulation cell (216 atoms, equivalent to 5000 appm defect concentration), they reevaluated their predictions. They found that the heat capacity and thermal expansion coefficients were little affected by the 0.5% defect concentration, in agreement with experimental data for neutron-irradiated SiC. In contrast, the thermal conductivity was markedly degraded by the dominant mechanism of defect scattering by phonons. The simulations predicted that the resulting conductivity would be essentially temperature independent from 1600K down to 436K. Interestingly, the relative conductivity degradation induced by the different types of point defects were ranked: Si interstitial at Tc site > Si antisite > C antisite > Si vacancy > C vacancy. For the 5000 appm defect concentration in β-SiC, the predicted thermal conductivity values ranged from about 15 up to 35 W/mK for the range of defect types listed above.

Listed in Table 2 for sample N3, the predicted concentration of radiation-induced defects is 4800 appm, which closely matches the 5000 appm defect concentration considered by Li, et al. However, at the irradiation temperature of 480°C the thermal conductivity calculated from the measured thermal diffusivity is only about 6.8 W/mK, more than a factor of two less than Li's conductivity predictions for any of the point defect types in SiC. An explanation for this discrepancy needs further investigation.

For engineering applications, the ratio of the irradiated to the unirradiated thermal conductivity values (k_{irr}/k_o) evaluated at the irradiation temperature is a useful quantity because k_{irr} represents the maximum degradation expected above saturation. Since neutron irradiation will have only a relatively small effect on the bulk density and heat capacity, $k_{irr}/k_o \approx \alpha_{irr}/\alpha_o$. This thermal diffusivity ratio was estimated for each irradiated CVD-SiC sample and is listed in Table 1. In Figure 2, the temperature dependence of k_{irr}/k_o is graphically presented for CVD-SiC, for the Hi-Nicalon™ and Sylramic™ composites reported earlier, and for similar values selected from the literature.

In Figure 2, the k_{irr}/k_o-data for CVD-SiC reported by Thorne, et al., Rohde, and Senor, et al. were similarly plotted in [11]. Likewise, k_{irr}/k_o-data for SiC/SiC composite made with first generation Nicalon™ CG fibers were given. The general trend is for the k_{irr}/k_o ratio to increase as the irradiation temperature increases. This trend reflects the relative dominance of temperature independent point defect phonon scattering in the lower temperature range, while the temperature dependent phonon-phonon scattering becomes relatively more important as the irradiation/test temperature increases. The curve for CVD-SiC represents the lower limit for irradiation degradation in SiC. In contrast, the phonon scattering in SiC/SiC composite materials is dominated by numerous structural defects even before irradiation, and the addition of irradiation point defects has a relatively small effect on the conductivity degradation. Thus, the curve through the Nicalon™ CG composite data marks an upper limit for the k_{irr}/k_o ratio for SiC-based materials. The new k_{irr}/k_o data for the SiC/SiC composite made with second generation Hi-Nicalon™ or Sylramic™ fiber generally fall in between the two limits.

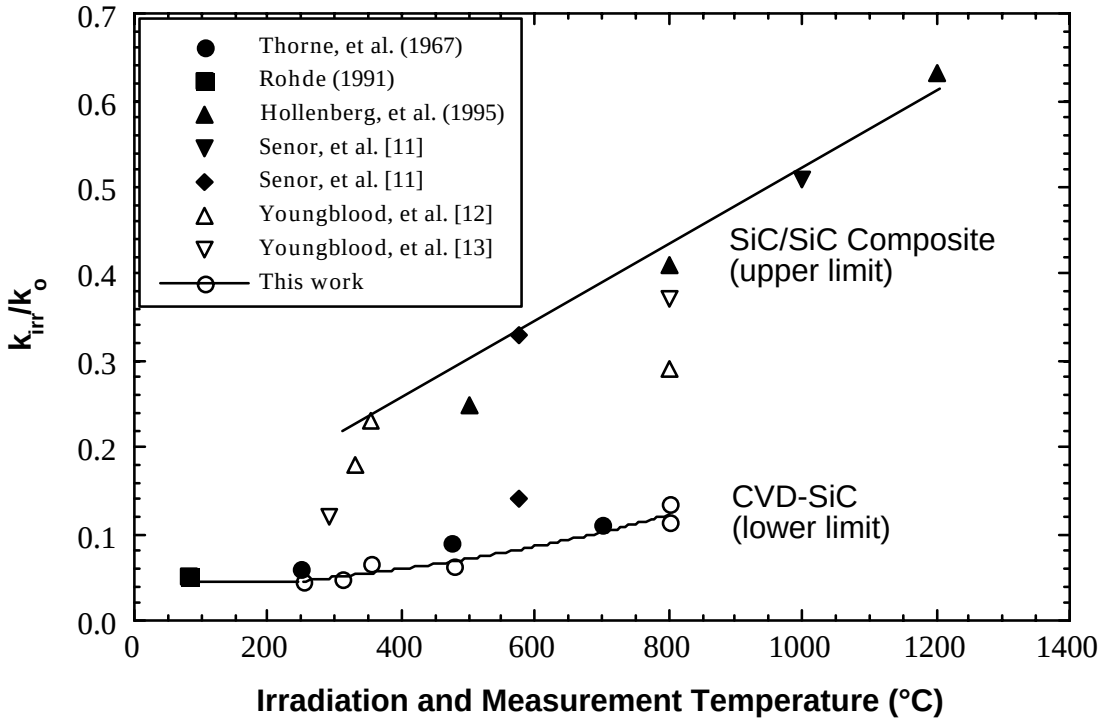

Figure 2. Conductivity degradation as a function of irradiation and test temperature for CVD-SiC and SiC/SiC composite.

FUTURE WORK

An attempt will be made to examine the kinetics of the thermal diffusivity recovery during annealing for the CVD-SiC samples irradiated at different temperatures and containing vastly different concentrations of point defects. Appropriate TEM analysis will accompany the thermal diffusivity recovery studies.

REFERENCES

[1] J. Price, "Annealing behavior of neutron-irradiated SiC temperature monitors," Nuclear Technology 16, 536-542 (1972).

[2] G. E. Youngblood, "Passive SiC irradiation temperature monitor," p. 324 in Fusion Materials Semiannual Progress Report (FMSPR) for period ending December 31, 1995. (DOE/ER-0313/19)

[3] G. E. Youngblood and W. Kowbel, "Improvements of the thermal conductivity of SiCf/SiC composite," p. 107 in *ibid*.

[4] Li, Lisa Porter and Sydney Yip, "Atomistic modeling of finite-temperature properties of crystalline β-SiC: II. Thermal conductivity and effects of point defects," J. Nucl. Mater. 255, 139-152 (1998).

[5] Morton Advanced Materials, 1996. CVD Silicon Carbide, technical Publication 107, Morton Advanced Materials (now Rohm and Haas), Woburn, MA 01801.

[6] D. R. Flynn, "Thermal conductivity of ceramics," p. 63 in Mechanical and Thermal Properties of Ceramics, ed. J. B. Wachtman, Jr., NBS Special Publication 303, Washington D.C., May, 1969.

[7] J. S. Haggerty and A. Lightfoot, "Opportunities for enhancing the thermal conductivities of SiC and Si3N4 ceramics through improved processing," Ceram. Eng. Sci. Proc., 475-487 (1996).

[8] D. J. Senor, G. E. Youngblood, D. V. Archer and C. E. Chamberlin, "Recent progress in thermal diffusivity testing of SiC-based materials for fusion reactor applications," p. 102 in the Proceedings of the 3rd IEA SiC/SiC Workshop, January 29-30, 1999, Cocoa Beach, Florida.

[9a] A. L. Qualls, "HFIR-MFE-RB-14J specimen loading listing and operational summary," p. 241 in FMSPR for period ending June 30, 2000. (DOE/ER-0313/28)

[9b] M. L. Grossbeck, K. E. Lenox and M. A. Janney, "The Monbusho/U.S. experiment: HFIR-MFE-RB-11J and 12J," p. 254 in FMSPR for period ending June 30, 1997. (DOE/ER-0313/22)

[10] S.J. Zinkle and L.L. Snead, "Thermophysical and mechanical properties of SiC/SiC composites," p. 93 in FMSPR for period ending December 31, 1998. (DOE/ER-0313/24)

[11] D. J. Senor, G. E. Youngblood, C. E. Moore, D. J. Trimble, G. A. Newsome and J. J. Woods," Effects of neutron irradiation on thermal conductivity of SiC-based composites and monolithic ceramics," Fusion Technology 30(3), 943-955 (1996).

[12] G. E. Youngblood, D. J. Senor and R. H. Jones, "Thermal diffusivity/conductivity of irradiated Hi-Nicalon™ 2D-SiC$_f$/SiC composite," in this FMSPR.

[13] G. E. Youngblood, D. J. Senor and R. H. Jones, "Thermal diffusivity/conductivity of irradiated Sylramic™ 2D-SiC$_f$/SiC composite," in this FMSPR.

EVALUATION OF TRANSTHICKNESS TENSILE STRENGTH OF SiC/SiC COMPOSITES - T. Hinoki, E. Lara-Curzio and L.L. Snead (Oak Ridge National Laboratory)

OBJECTIVE

The objective of this work is to develop experimental technique for measuring transthickness tensile strength using diametral compression and to understand usability of the experiment and specimen size effect.

SUMMARY

The transthickness tensile strength (TTS) of 2-D CVI-SiC/SiC composites reinforced with Tyranno SA fibers was evaluated by the diametral compression test. The effects of specimen size and specimen shape on the magnitude of the TTS were studied and the results were analyzed using an analysis of variance (ANOVA) and Weibull statistics.

Specimens failed along an interlaminar plane adjacent to the line of action of the applied load and fractographic analyses revealed that the crack had propagated through matrix pores and along interfaces between the fiber, fiber coating and matrix. The magnitude of the TTS was found to be independent of specimen size or shape for the range of specimen dimensions investigated, although the amount of scatter was largest for the results obtained from the evaluation of the smallest specimens. The characteristic value of the TTS and the Weibull modulus for the distribution of TTS values were 24.9 MPa and 6.48, respectively.

PROGRESS AND STATUS

Introduction

SiC/SiC composites are considered for use in extremely harsh environments primarily due to their excellent thermal, mechanical and chemical stability, and the exceptionally low radioactivity following neutron irradiation [1-2]. In particular, recent improvement in the crystallinity and purity of SiC fibers, the developments and improved composite processing have improved physical and mechanical performance under harsh environments [3-5]. The tensile strength perpendicular to the lay-up planes of 2D laminated composites (transthickness tensile strength: TTS) is typically much lower than the strength of the composite on the lay-up plane. Therefore, it is likely that the design of engineering components utilizing these materials will be limited by strength in this direction. Recently, the American Society for Testing and Materials (ASTM) standardized test method C1468 to evaluate the TTS of continuous fiber-reinforced ceramic matrix composites (CFCCs). Because this test method relies on the use of adhesively-bonded extenders to transfer load to the specimen, its applicability is limited by the properties of the adhesive and can only be used at low temperatures. The diametral compression test [6-9], also known as Brazilian test, overcomes the limitations imposed by the adhesive and, therefore, can be applied at high temperatures. This test method is based on the fact that tensile stresses develop when a circular disk is compressed by two diametrically opposed forces as shown in Fig. 1. These tensile stresses exist perpendicularly to the loading direction and are proportional to the applied compressive force. The preparation of test specimens and the actual tests are relatively straightforward, making this test method

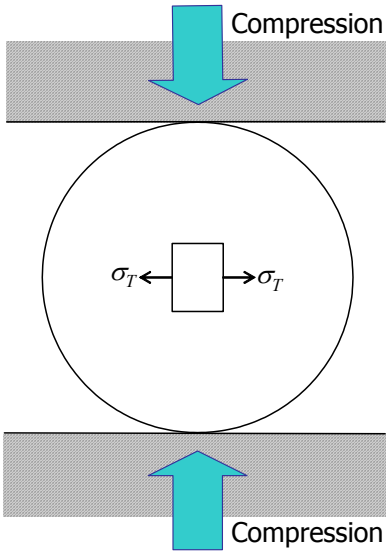

Fig. 1: Transthickness tensile strength by diametral compression

amenable for use. Because of these reasons, this test method is currently being considered for ASTM standardization.

In this paper we report the TTS results from the evaluation of a 2-D SiC/SiC CFCC by diametral compression. The effects of specimen size and shape on the magnitude of the TTS were investigated and the results were analyzed using Weibull statistics. A discussion regarding the determination of the TTS from the magnitude of the applied load and specimen dimensions is also included.

Experimental

The material used in this investigation consisted of plain-weave Tyranno™ SA fabric, stacked in [0°/90°] direction, and a SiC matrix synthesized by forced-flow thermal-gradient chemical vapor infiltration [10]. A dual coating of approximately 80 nm-thick SiC and 570 nm-thick C was applied to the fiber prior to matrix infiltration. Pieces with 75 mm diameter and 12.5 mm thick were obtained with 22.6 % porosity. Details of the material and its fabrication can be found elsewhere [6]. Disk specimens of various sizes (diameter: 3.2, 6.4, 9.4 mm, thickness: 1.7, 3.1, 4.5, 6.0 mm) were obtained from the composite piece by core-drilling using a diamond-impregnated tool. Truncated disk specimens (diameter: 6.5 mm, thickness: 3.1 mm, width: 3.2 mm) were also obtained as illustrated in Fig. 2.

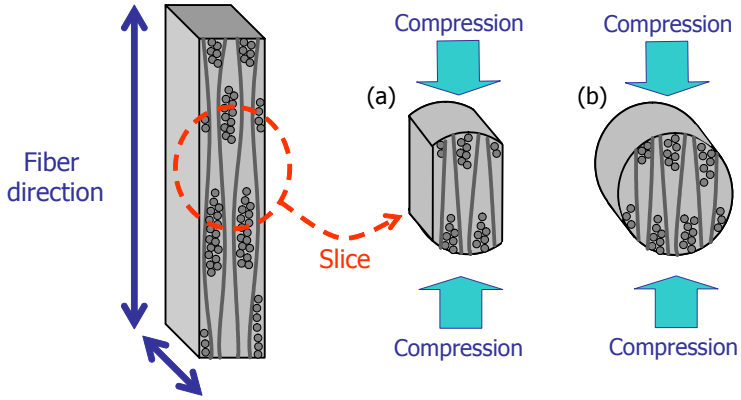

Fig. 2: Specimen types for diametral compression tests, (a) truncated disk, (b) disk

Transthickness tensile tests were carried-out at ambient conditions (20°C/35% RH) using an electromechanical testing machine at a constant cross-head displacement rate of 10 μm/s. The test specimens were subjected to diametral compression using two parallel plates of Hexoloy® SA SiC. This material was selected due to its low Poisson's ratio (0.14) and high elastic modulus (390 GPa) to minimize radial expansion at the contact area. The specimens were aligned and fixed with double-sided tape on the bottom plate. Fig. 2 illustrates the relation between the fabric orientation and the loading direction. At the end of the tests, the fracture surfaces were examined by scanning electron microscopy.

Result and discussion

Fig. 3 shows typical stress-displacement curves for specimens of various sizes. In every case the load increased monotonically to a peak value, which was followed by an abrupt drop and an audible indication that the sample had failed. Every specimen failed by a crack that propagated along the loaded diameter, along an interlaminar region through large pores in the matrix, and along the fiber/fiber coating/matrix interfaces. Fig. 4 is an SEM micrograph of a typical fracture surface. Debonded fibers and CVI coated fiber-bundle surfaces without matrix infiltration were evident on the fracture surfaces.
The TTS (σ_T) was determined according to Eq. (1).

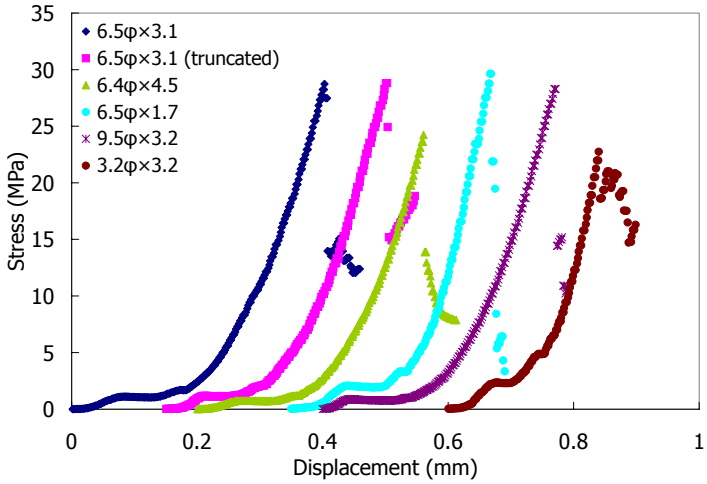

Fig. 3: Typical loading curves of various size specimens

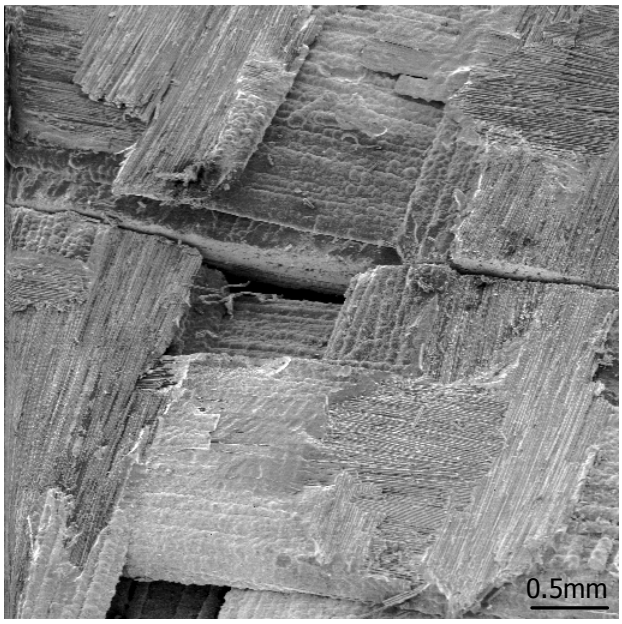

Fig. 4: Fracture surface after the diametral compression test

$$\sigma_T = \frac{2P}{\pi dt} \qquad (1)$$

where *P* is the load at failure, *d* is the diameter, and *t* is the thickness of the specimen [7,8]. However, this relationship between the TTS and the failure load is only valid for isotropic materials and, therefore, it needs to be corrected to account for the transverse isotropy of the material evaluated. This work is in progress and will be reported in the future.

Fig. 5(a) shows the effect of diameter on the TTS of SiC/SiC test specimens 3.1 mm-thick, while Fig. 5(b) shows the effect of thickness on the TTS of SiC/SiC 6.5 mm-diameter test specimens. The error bars represent one standard deviation about the mean value. In the thickest specimens, it was difficult to identify the magnitude of the load at which failure ocurred, since the curves showed multiple load drops. Two values of TTSs were obtained for these specimens from two critical loads in the curves. An analysis of variance (ANOVA) [11] of all the test results revealed that there are no significant differences among these mean

values at the 95 % confidence level. Therefore, for the range of values examined, there are no apparent size effects on the magnitude of the TTS of the material evaluated. It was found, however, that scatter was largest for the TTS values obtained with small-diameter (3.2 mm) specimens, which can be attributed to lack of precision in the alignment of the test specimen during the test, and the reduced number of fabric unit cells in the gauge section of the test specimen.

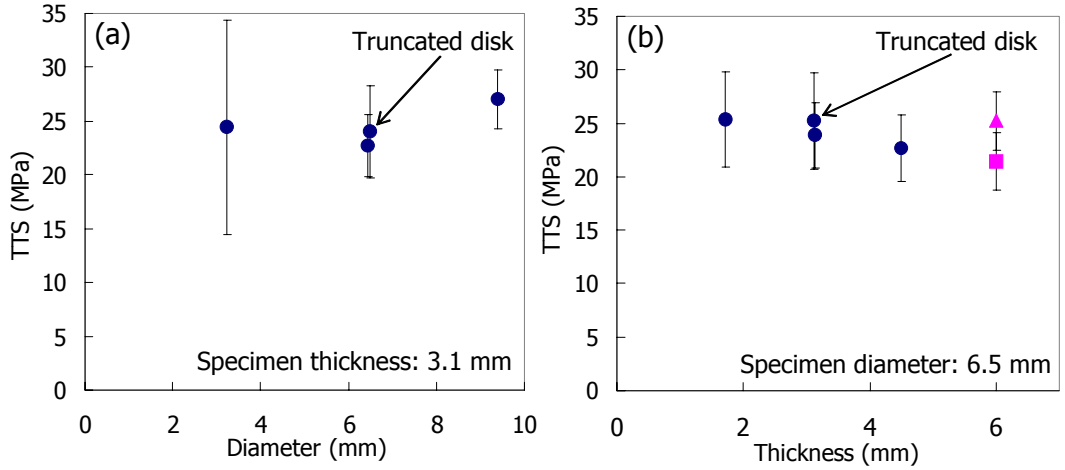

Fig. 5: Size effects on transthickness tensile strength, (a): effect of diameter, (b): effect of thickness

The TTS results were analyzed using Weibull statistics. Fig. 6 shows Weibull plots for (a) TTS of standard size specimens (diamter: 6.4 mm, thickness: 3.1 mm); (b) TTS of all specimens without the thickest specimens (thickness: 6.0 mm). The Weibull modulus and scale parameter for the standard specimens are 9.41 and 25.1 MPa, respectively, while those for the entire data set are 6.48 and 26.7 MPa, respectively. The Weibull modulus of the strength data set that includes all specimens is smaller than that of standard size specimens, and this is attributed to the large scatter of the data obtained from the evaluation of small diameter specimens. The Weibull modulus for a data set that excludes the small diameter specimens is 8.15. This relatively large value of the Weibull modulus is consistent with materials that contain large-sized defects that are responsible for failure.

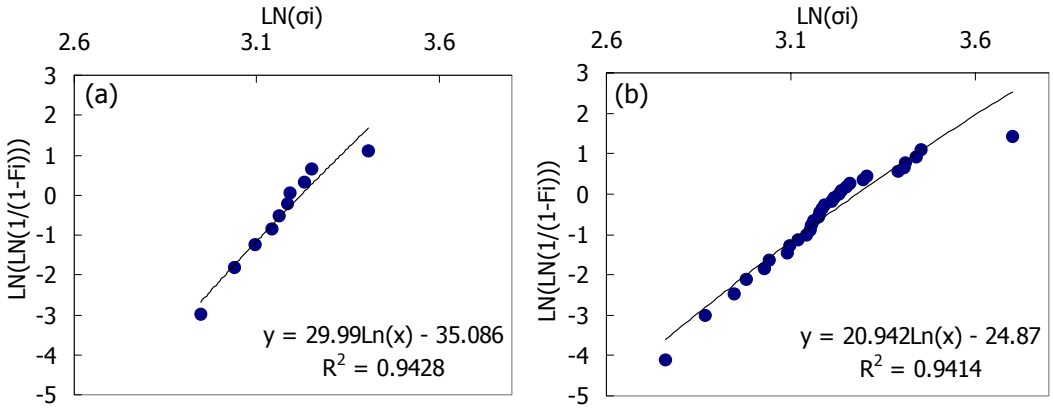

Fig. 6: Weibull plots of transthickness tensile strength of (a): standard size specimens and (b): all specimens

It was also found that the TTS of the material evaluated was independent of specimen geometry, i.e.- disk-shaped versus truncated disk-shaped specimens. This is important because for the range of dimensions investigated in this work, these results validate the use of truncated-disks specimen geometries when the material is available only as a thin plate and the diameter of the disk is larger than the thickness of the plate. Therefore, these results support the validity of this test method for the evaluation of the

transthickness tensile strength of 1-D and 2-D CFCCs.

CONCLUSION

The TTS of CVI-SiC reinforced with Tyranno™ SA fibers was evaluated by diametral compression using specimens of various sizes (diameter and thickness) and shapes (disks vs. truncated disks). All specimens failed along an interlaminar plane adjacent to the diametral plane of the applied load. Analysis of the fracture surfaces revealed that the dominating crack grew along large pores in the matrix and along the fiber/fiber coating/matrix interfaces. It was found that for the range of specimen dimensions investigated, the magnitude of the TTS was independent of size or specimen geometry (disk vs. truncated disk). It was also found that there was considerable scatter in the TTS results obtained from the evaluation of the smallest disk specimens, and this could be attributed to reduced precision in the alignment of the specimen during the test, and the reduced number of fabric unit cells in the gauge section. The average TTS, the one standard deviation, the Weibull modulus and the scale parameter for the entire data set were 24.9 MPa, 4.77, 6.48 and 26.7 MPa, respectively. Although the magnitude of TTS was determined from the peak load using the elastic solution for isotropic materials and, therefore, needs to be corrected to account for the transverse isotropy of the material, these results demonstrate the applicability of this test method to determine the TTS of CFCCs. On-going work is focused on the determination of correction factors to account for anisotropy and the implementation of this test method at elevated temperatures.

ACKNOWLEDGEMENTS

The material used in this work was fabricated under the collaboration program of Oak Ridge National Laboratory, Japan Atomic Energy Research Institute, and Kyoto University. This work was supported by the office of Fusion Energy Science, US DOE under contract DE-AC-05-00OR22725 with UT-Battelle, LLC.

REFFERENCES

[1] A. Kohyama and Y. Katoh, Ceramic Transactions, 144 (2002) 3-18.
[2] L.L. Snead, R.H. Jones, A. Kohyama and P. Fenici, J. Nucl. Mater., 233-237 (1996) 26-36.
[3] M. Takeda, A. Urano, J. Sakamoto and Y. Imai, J. Nucl. Mater., 258-263 (1998) 1594-1599.
[4] T. Ishikawa, S. Kajii, T. Hisayuki, K. Matsunaga, T. Hogami and Y. Kohtoku, Key Eng. Mater., 164-165 (1999) 15-18.
[5] T. Hinoki, L.L. Snead, Y. Katoh, A. Hasegawa, T. Nozawa and A. Kohyama, J. Nucl. Mater., 307-311 (2002) 1157-1162.
[6] A. Okada, J. Mater. Sci., 25 (1990) 3901-3905.
[7] S. P. Timoshenko and J. N. Goodier, Theory of Elasticity, McGraw-Hill, NY (1970)
[8] T.V. Parry and A.S. Wronski, J. Mater. Sci., 25 (1990) 3162-3166
[9] T. Hinoki and E. Lara-Curzio, 104th annual meeting of Am. Ceram. Soc., St. Louis, Apr., 2002.
[10] T. Hinoki, L.L. Snead, T. Taguchi, N. Igawa, W. Yang, T. Nozawa, Y. Katoh and A. Kohyama, Ceramic Transactions, 144 (2002) 55-68.
[11] R.L. Scheaffer and J.T. McClave, Statistics for Engineers, PWS Publishers, Boston, (1982).